

August 9, 2018

Stellar Activity on the Young Suns of Orion: COUP Observations of K5-7 Pre-Main Sequence Stars

S.J. Wolk and F.R. Harnden Jr.¹

Harvard-Smithsonian Center for Astrophysics, 60 Garden Street, Cambridge, MA 02138

`swolk@cfa.harvard.edu`

E. Flaccomio & G. Micela

*INAF - Osservatorio Astronomico G.S. Vaiana - Piazza Parlamento I, 90134 Palermo,
Italy*

F. Favata

*Astrophysics Division – Research and Space Science Support Department of ESA, ESTEC,
Postbus 299, NL-2200 AG, Noordwijk, The Netherlands*

H. Shang

Institute of Astronomy and Astrophysics, Academia Sinica, Taiwan

and

E.D. Feigelson

*Department of Astronomy & Astrophysics, Pennsylvania State University, University Park,
PA 16802*

ABSTRACT

In January 2003, the *Chandra* Orion Ultradeep Project (COUP) detected about 1400 young stars during a 13.2 day observation of the Orion Nebula Cluster (ONC). This paper is a study of the X-ray properties of a well-defined sample of 28 solar-mass ONC stars based on COUP data. Our goals are to characterize

¹Universe Division, Science Mission Directorate NASA Headquarters

the magnetic activity of analogs of the young Sun and thereby to improve understanding of the effects of solar X-rays on the solar nebula during the era of planet formation. Given the length of the COUP observation we are able to clearly distinguish characteristic and flare periods for all stars. We find that active young Suns spend 70% of their time in a characteristic state with relatively constant flux and magnetically confined plasma with temperatures $kT_2 \simeq 2.1 \times kT_1$. During characteristic periods, the 0.5 – 8 keV X-ray luminosity is about 0.03% of the bolometric luminosity. One or two powerful flares per week with peak luminosities $\log L_x \sim 30 - 32$ ergs s^{-1} are typically superposed on this characteristic emission accompanied by heating of the hot plasma component from $\simeq 2.4$ keV to $\simeq 7$ keV at the flare peak. The energy distribution of flares superposed on the characteristic emission level follows the relationship $dN/dE \propto E^{-1.7}$. The flare rates are consistent with the production of sufficiently energetic protons to spawn a spallogenic origin of some important short-lived radionuclides found in ancient meteorites. The X-rays can ionize gas in the circumstellar disk at a rate of 6×10^{-9} ionizations per second at 1 AU from the central star, orders of magnitude above cosmic ray ionization rates. The estimated energetic particle fluences are sufficient to account for many isotopic anomalies observed in meteoritic inclusions.

Subject headings: Sun: activity - meteors, meteoroids - open clusters and associations: individual (Orion Nebular Cluster) - stars:activity - stars: pre-main sequence- X-rays: stars

1. Introduction

The formation of stars and their planetary systems is generally viewed as a low temperature phenomenon. Dark molecular cores at $T \sim 10$ K collapse to pre-main sequence (PMS) stars with surfaces at $T \sim 10^3$ K surrounded by dusty disks with characteristic temperatures of $T \sim 10^2$ K. These earliest stages of stellar evolution are studied primarily in the millimeter through optical bands. Most efforts to understand the astrophysics of these stages treat gravitational, hydrodynamical and chemical processes of neutral molecular material in gaseous and solid forms.

However, three lines of evidence point to the presence of higher energy phenomena in young stellar systems, ranging from excited gas at temperatures of $T \sim 10^4$ K, to highly-ionized plasma at $T \sim 10^7$ K, to particles accelerated up to $kT \sim$ MeV energies:

1. Low-excitation emission line gas, which dominates the optical spectra of T Tauri stars and was formerly attributed to hot outflowing winds, is now commonly thought to arise in magnetically funneled accretion from the circumstellar disk (see review by Hartmann 2001). To conserve angular momentum, the accretion is accompanied by ejection of disk material in magnetically collimated jets seen as Herbig-Haro outflows (Shu et al. 2000).
2. X-ray emission is ubiquitous in PMS stars at levels that are orders of magnitude above those seen in most main sequence stars. These PMS stars generally show high-amplitude rapid variability and the type of hard spectra that are associated with violent magnetic reconnection flares when seen on the surface of the Sun, dMe flare stars and other magnetically active late-type stars (Feigelson & Montmerle 1999, Favata & Micela 2003, Güdel 2004).
3. Studies of the isotopic composition of components of ancient meteorites require either the injection of short-lived nuclides into the molecular cloud that formed our solar system, or *in situ* irradiation of solids by MeV baryons in the solar nebula (Goswami & Vanhala 2000). Radio observations show gyrosynchrotron radiation from MeV electrons accelerated by magnetic flares in some young stellar systems (Güdel 2002).

Together, these studies indicate that astrophysical modeling of young stellar systems, and particularly their protoplanetary disks, requires treatment of ionization, nuclear spallation, and magnetohydrodynamical processes in addition to processes affecting neutral materials (see reviews by Feigelson & Montmerle 1999, Glassgold, Feigelson, & Montmerle 2000; hereafter GFM00, Feigelson 2005 and Glassgold et al. 2005). High-energy photon and particle irradiation of protoplanetary disks may substantially alter the thermal, chemical, ionization, and dynamical (e.g., laminar *vs.* turbulent flow) state of the disk. Long-standing mysteries in solar nebula studies, such as the flash melting of meteoritic chondrules and the presence of short-lived radionuclides, may be explained, at least in part, by these high energy phenomena in young stellar systems. Planet formation and early evolution such as inward migration should be substantially different in an irradiated disk as compared to an isolated disk.

Disk solids will be affected both by the observed X-rays and by other high energy manifestations of the violent magnetic connection process that heats the X-ray emitting plasma. These flare events should produce shock fronts analogous to solar coronal mass ejections (CMEs) accompanied by baryons and electrons accelerated to MeV energies. For example, the solar X17 flare of 28 Oct 2003 produced a peak fluence of 8×10^5 protons $\text{cm}^{-2} \text{s}^{-1} \text{ster}^{-1} \text{MeV}^{-1}$ around 1 keV and 8×10^4 protons $\text{cm}^{-2} \text{s}^{-1} \text{ster}^{-1} \text{MeV}^{-1}$ around

1 MeV, as measured by the Advanced Composition Explorer. This represents a rise of a factor of 10^4 in particle fluence from the quiescent level and was accompanied by a 10^3 -fold outburst in X-ray emission with peak X-ray luminosity $L_x \simeq 4 \times 10^{27}$ erg s $^{-1}$ seen with the GOES 12 satellite. When scaled upward to the $10^{28} - 10^{32}$ ergs s $^{-1}$ flares seen in T Tauri stars surrounded by protoplanetary disks, the inferred X-ray or shock wave heating may flash melt chondrules (Shu et al. 2001, Nakamoto et al. 2005) and the inferred MeV particle fluence may produce anomalous abundances of short-lived radionuclides seen in Ca-Al-rich inclusions (CAIs) of ancient carbonaceous chondritic meteorites (Feigelson 1982, Gounelle et al. 2001, Goswami, Marhas & Sahijpal 2001, Leya, Halliday & Wieler 2003).

The study of the effects of high energy products of magnetic flares on young circumstellar disks is being propelled by observations with the *Chandra X-ray Observatory* with its large collecting area and elliptic orbit that permits long continuous exposures. The VLA radio telescope also provides direct measurements of gyrosynchrotron emission from MeV electrons in some young stars (Güdel 2002). Feigelson, Garmire, & Pravdo (2002; henceforth FGP02) investigated the X-ray flaring of a complete sample of 43 solar-mass stars in the Orion Nebula Cluster (ONC) observed with *Chandra's* Advanced CCD Imaging Spectrometer (ACIS) in two ~ 12 -hour exposures during 1999-2000. They found that solar analogs with ages ≤ 1 Myr exhibit flares $\simeq 30$ times more powerful and $\simeq 300$ times more often than the most powerful flares on the contemporary Sun and argued that such flares imply factors of 10^5 enhancement in the MeV proton fluence from the young Sun. They conclude that this is sufficient to explain some of the important CAI isotopic anomalies by *in situ* spallation reactions.

The present paper continues this effort to measure flaring properties of young solar analogs directly and understand the impact on protoplanetary disks. The principal goal of this study is to obtain quantitative measures of the variability, particularly the impulsive flaring, of pre-main sequence analogs of our Sun. We establish the frequency, duration and energetics of flaring, and strive to understand their effects on the protoplanetary disks that surround many of these stars. We then study the effect of the flares on the disk. Our paper is based on a nearly continuous observation of the ONC made with *Chandra's* ACIS detector over a 13.2-day period in January 2003. Known as the *Chandra* Orion Ultradeep Project (COUP), this observation provides the most comprehensive database for studies of young stellar X-rays and magnetic activity (Getman et al. 2005; henceforth G05).

Due to strong dependencies of X-ray luminosity on stellar mass (Preibisch et al. 2005a), we limit this study to stars with masses close to $1.0 M_{\odot}$. Section 2 defines the sample, §3 describes our extraction of flares from the complex X-ray light curves, and §4 outlines our spectral analysis procedures. Results on the X-ray intensities, durations, frequencies, ener-

getics and dependencies on stellar age and disk properties are presented in §5. Implications for effects of protoplanetary disk gases and solids are outlined in §6.

2. Selection of Sources

The COUP observation, field of view, X-ray source detection, event extraction, X-ray properties and stellar counterparts are described in detail by G05, who give extensive tables of source properties. The present paper gives a close examination of the subset of COUP sources with masses $0.9 < M < 1.2 M_{\odot}$, which is roughly in the mass range of F7-G5 stars on the Zero Age Main Sequence (ZAMS). This selection permits comparison with samples of ZAMS G stars from the Pleiades, Hyades and other stellar samples (Preibisch 2005b).

Twenty-eight COUP sources in Table 9 of G05 and two undetected stars in their Table 11 have masses in the desired range giving a total sample size of 30 stars for our study. These sources are shown on the COUP and 2MASS fields in Figure 1. These masses were derived in G05 by applying the evolutionary tracks of Siess, Dufour, & Forestini (2000; henceforth SDF00) to stellar positions in the Hertzsprung-Russell diagram derived from optical spectroscopy and photometry of $V < 20$ ONC stars by Hillenbrand (1997) [as updated in G05]. Choices of mass tracks and spectral type to temperature conversions used in G05 were made to maximize utility and were not optimized for a particular study. The sample used here differs from that obtained by FGP02, who also used the HR Diagram of Hillenbrand (1997) but applied the theoretical tracks of D’Antona & Mazzitelli (1997; henceforth DM97). The SDF00 calculations have different treatments of degenerate electron pressure, chemical composition and mixing length parameter from those of DM97 tracks. While the two sets tracks show similar performance with respect to dynamically measured masses (Hillenbrand & White 2004), the SDF00 tracks were selected in G05 for their applicability to a wider range of masses for the full COUP study.

How well the stars selected here truly represent “young Suns” depends strongly on the ability of models to predict accurate masses from temperatures and luminosities and upon limitations in measuring those quantities. Compared to the DM97 tracks, the SDF00 tracks predict surface temperatures up to 600 K cooler and higher luminosities for $\simeq 1 M_{\odot}$ stars along the convective Hayashi tracks. Consequently, for a given luminosity the SDF00 age estimate is younger and the mass estimate is higher. The masses range from 10% to 100% increases over those predicted by DM97. The result is that most of the 30 stars considered here lie below the $0.8 - 1.4 M_{\odot}$ range considered by FGP02 – only 7 stars are in common between the two samples. The samples would have more closely overlapped had we considered the $1.2 < M_{\odot} < 1.4 M_{\odot}$ SDF00 mass range.

Another selection effect implicit in the use of the Hillenbrand (1997) spectroscopic sample is the omission of heavily obscured ONC stars. The highest extinction in our subsample is $A_V \approx 6.3$. Thus, we exclude a number of obscured stars whose location in the $K - (H - K)$ diagram (see e.g., Hillenbrand & Carpenter 2000) predicts a mass around $1 M_\odot$. We also omit the weak-lined T Tauri star GMR-A with $A_V \simeq 35$ and an inferred mass slightly over $1 M_\odot$; it exhibited extraordinarily powerful radio and X-ray flares during the COUP observation (Bower et al. 2003). Again, we believe that the omission of high- A_V stars from consideration will have little or no effect on our conclusions regarding magnetic activity of solar analogs. It has the further advantage that soft X-ray absorption in our sample is never very strong with column densities $\log N_H \leq 22.0 \text{ cm}^{-2}$.

Table 1 lists measured optical and near-infrared properties of the sample stars, and Table 2 gives inferred properties such as effective temperature $\log T_{eff}$, bolometric luminosity $\log L_{bol}$, radius R , mass M , age t , in addition to the K -band excess ($\Delta(I - K)$) and the equivalent width of the Ca II triplet. We do not tabulate the errors in the table for clarity, but they can be significant. A recent analysis by Hillenbrand & White (2004) found that PMS stars of about $1M_\odot$ have luminosity errors of about 0.1 dex. This reflects typical spectral subclass errors (of one subclass), photometric errors introduced both by observational error (less than 3%), variability and extinction (errors of $< 10\%$). The choice of a particular PMS evolutionary mass model will introduce a bias in source selection. Hillenbrand & White found that the DM97 and SDF00 models both systematically underestimate sub-solar masses by 10%–30% on average, with scatter of the same order. Further, we note the very non-uniform mass distribution among the sources listed in Table 2: only one source lies between 0.95 and $1.09 M_\odot$. This is caused by the quantization of temperature to 200 degree increments (0.02 dex in $\log T$) by G05. A temperature difference of 200K corresponds to $0.2 M_\odot$ along the convective part of the evolutionary track in these models. This limitation of the dataset quantizes sample masses somewhat and results in a systematic shift in the attributed mass of stars, with masses between 1.3 – $1.0 M_\odot$ shifting toward $1.12 M_\odot$, and masses between 1.0 – $0.8 M_\odot$ shifting toward $0.90 M_\odot$. We cannot limit the mass selection as tightly as we had hoped for stars younger than about $\log 6.5$ yrs, but we believe these issues have little effect on our conclusions, other than shifting slightly downward the average X-ray luminosities as compared to FGP02 (see also Preibisch 2005a).

All quantities in Table 1 are obtained from the tables of G05 where a full description of their derivation is given. Throughout this paper, we refer to sources by their COUP number which ranges from 1 – 1616. The corresponding optical identifier is the star number in Jones and Walker (1988). There is virtually no uncertainty in the association of COUP and bright optical ONC stars as the astrometric offsets are typically $< 0.2''$ (Table 1, columns 3-4), although contributions to both optical and X-ray flux by lower mass close binary companions

may be present. In two cases, the optical field shows a visual double where only the brighter component is associated with the COUP source.

Table 3 gives time-averaged X-ray luminosities selected from Tables 4 and 8 of G05. Column 2 gives the number of extracted counts (NetCts) from the position-dependent source region, after background-correction. Columns 3–6 give time-averaged luminosities in three bands – $\log L_s$ in the soft 0.5 – 2 keV band, $\log L_h$ in the hard 2 – 8 keV band, and $\log L_t$ in the total 0.5 – 8 keV band – and the absorption-corrected intrinsic total band luminosity $\log L_{t,c}$. The final column lists notes about each source.

Note that the two solar analog stars that were **not** detected by the COUP (from Table 11 in G05), JW 252 and JW 407, are both close to other bright COUP sources which raised the local background. JW 252 has estimated mass of $1.18 M_\odot$ and an age of 2.5 Myr but lies in the wings of COUP 222 associated with JW 256 lying $3.8''$ to the NE. JW 407 has estimated mass of $0.91 M_\odot$ and an age of 2.0 Myr but lies $3.4''$ to the ESE of and in the wings of COUP 520. COUP 520 is not associated with an optical source but is associated with 2MASS 05351317-0517307 with an offset of $< 0.15''$. These stars are probably not qualitatively different from the resolved sources, and will not be further discussed in this paper.

In all but four cases, the optically-derived visual absorptions A_V agree with the X-ray-derived column densities $\log N_H$ given the conversion $N_H = 1.6 \times 10^{21} A_V \text{ cm}^{-2}$ obtained by Vuong et al. (2003). COUP 241, 314 and 1167 are discrepant in that they exhibit almost no counts below 0.8 keV and thus have high inferred $\log N_H$ value, inconsistent with the low reported A_V . COUP 1539 is discrepant in the other direction possibly due to an unusually soft X-ray flare.

We estimate that about half of the COUP-detected solar mass ONC stars possess circumstellar disks based on three criteria. First, three stars have proplyds, disks imaged in silhouette against the bright nebula or imaged in $H\alpha$ emission by the *Hubble Space Telescope*. An additional 13 stars appear to have inner dusty disks producing K -band excesses $\Delta(I - K) > 0.3$ over the emission expected from an isolated photosphere. Third, three of these sixteen stars show significant Ca II triplet emission, $\text{EW}(\text{Ca II}) \leq -3\text{\AA}$, which is a rough indicator of accretion (Flaccomio et al. 2003, Sicilia-Aguilar et al. 2005).

3. Definition of a Flare

The distinguishing aspect of the COUP dataset is the unprecedented duration of nearly continuous observation. This allows a unique perspective of the temporal behavior of the X-

ray sources. While flaring is ubiquitous among coronal X-ray sources, the temporal behavior of X-ray sources is complex. Separating obvious flares and less obvious periods of variable emission, determining “quiescent” flux levels and quantifying the intensities of flaring have all been challenges.

3.1. Quantifying Variability

Several groups have used different techniques to quantify variability in stellar X-ray sources. Observations of stars by ROSAT were typically divided into fairly short observation intervals (OBIs) of order 3 ks. This prevented observation of flares from beginning to end but allowed observers to easily compare count rates among various OBIs and often define flares as the doubling of flux in one OBI as compared to another. A more rigorous technique commonly used is a one-sample Kolmogorov-Smirnov (KS) test, but virtually every X-ray source (star or otherwise) varies if observed for a sufficient duration and with sufficient sensitivity. G05 reports that 974 of 1616 X-ray sources in the COUP data set were non-constant at a confidence level of greater than 99%. The solar mass stars discussed here are all non-constant at a confidence of 99%.

There is a plethora of other methods that have been used to determine variability. These methods include: distribution of binned count rate (Saar & Bookbinder 1998, Güdel 2003), $n - \sigma$ deviation from the mean (Stelzer et al. 2000, Wolk et al. 2004), Lagrange multipliers (Schwartz 1987), Poisson tests (e.g., Maccacaro et al. 1987), avalanche and cellular automata models (Lu & Hamilton 1991, Lu 1995), phase space reconstruction (Vio et al. 1992), KS visualization (Giommi et al. 1995), wavelet analysis (Aschwanden et al. 1998; Walker et al. 2000; many others), Poissonian structure function (Fernandes et al. 2000), time-frequency analysis (Vio & Wamsteker 2002) and combined K-S/ χ^2 criteria (Fuhrmeister & Schmitt 2003). We sought a method that is not only independent of data binning but also identifies blocks of data in a specific, not statistical sense.

We have chosen to employ a method to determine periods of constant signal similar to the Bayesian Block method discussed by Scargle (1998) and used in G05. The Bayesian Block technique segments the lightcurve into a sequence of constant brightness levels under the assumption of Poisson errors in the signal. The change points between levels are established using an iterative maximum likelihood procedure based on Bayesian principles. This method is explicitly designed to avoid binning of the observation into equally spaced time intervals. Bayesian Blocks do characterize the X-ray lightcurves remarkably well. As discussed in G05, the overall shape and number of Bayesian Blocks is fairly insensitive to the choice of confidence level.

We adopt here a procedure very similar to Bayesian Blocks but without use of Bayes’ Theorem. The sequence of constant brightness levels is established by maximizing likelihoods under the Poisson model in the same way, but our thresholds for establishing change points seek to minimize false positives to reduce fragmentation of Blocks into many small intervals. These thresholds were established from extensive simulations of constant lightcurves at different count rates. We call our procedure, used both here and in other COUP studies, Maximum Likelihood Blocks (MLB).

Further, we have made an attempt to overcome one of the main limitations of the Scargle method – the fact that it segments a light curve in only two segments at a time (the algorithm is then run recursively on each of the segments found). This is a limitation especially for finding faint impulsive events (e.g., flares), as a two segment representation in which one segment includes the event might not be statistically significant so that the segmentation process cannot start. For this reason, our code tests both the two- and the three-segment hypotheses. For computational efficiency, only segments with < 2000 counts are tested for the 3-segment hypothesis.

We found that using one count per average segment occasionally produced too many short blocks. For analysis in this study, the two parameters of the MLB algorithm were set to require a minimum of 20 counts per block and a 95% probability for establishing change points. For other COUP studies (e.g., involving much fainter sources), other parameters may be chosen. The median¹ observation in our sample contains 12 such blocks, five being the smallest number of blocks and 31 being the largest. The existence of multiple blocks tells us that the flux rate from all sources is non-constant at high confidence, but the number of blocks alone does not tell us anything about the type or level of activity detected.

3.2. The Morphology of Stellar X-ray Variability

Solar and stellar activity is often characterized in terms of “quiescent” versus “flaring” state. The latter state is sometimes divided into macroscopic distinct events and the superposition of many microflares or nanoflares. We consider only macroscopic flaring in this study. Although many COUP lightcurves exhibit frequent long roughly-constant periods of weaker emission between powerful flares, the term “quiescent” (dictionary definition: “marked by inactivity”) is a misnomer because the absolute activity level is often extremely

¹In this paper, we will generally quote the median not the mean since the median is insulated from outliers that can be the result of poor fits or low counts. When a dispersion is needed, we report the median absolute deviation (MAD; Beers et al. 1990).

high; e.g., $\log(L_t/L_{bol}) \simeq -4$ in contrast to -6 for the quiet Sun. We thus chose the term “characteristic” level to describe the typical emission between isolated flare events from a COUP star. We term the single flux block of weakest emission as the “Minimum Observed LLevel” (MOLE).

Upon subjective examination, the blocks divided themselves into three types: I) The **characteristic** level and blocks statistically compatible with the characteristic level. II) Periods of flux “elevated” above the characteristic level with no impulsive morphology. III) Periods of **elevated** flux marked by very rapid rises. We refer to only the third group as “**flares**,” this was the only group exhibiting consistent morphology. Specifically, all the events in group III showed either “classic” flare morphology (i.e., a fast rise followed by an exponential decay) or a symmetric morphology similar to that seen during EUVE observations of HR 1099 (Osten & Brown 1999). We also found it useful to define an intermediate “**very elevated**” level for unusually strong emission without rapid flux changes.

The classification of X-ray variations from our MLB segmentation of the COUP lightcurves is illustrated in Figure 2 for COUP 567. The top panel shows the binned lightcurve overlaid with the 25 MLBs used in our analysis.

Characteristic Level – We established the characteristic level iteratively, first identifying the set of blocks that maximize the period of time covered by compatible blocks. A segment is deemed compatible with count rate, R , if its count rate, $R_{block} \pm \sigma$, is between $R/1.2-1.5\sigma$ and $R*1.2+1.5\sigma$. Here, σ is the standard deviation of the observed rate about the mean rate in the block. A reference count rate R_{ref} is defined as that rate for which the compatible time reaches a maximum. Then characteristic segments are re-selected to include

$$R_{block} < 1.2 \times R_{char} + 1.5\sigma \tag{1}$$

Although there are cases in which it is very difficult, even for the eye, to define a characteristic level, this algorithm gives reasonable results. In the middle panel of Figure 2 there are 11 characteristic MLBs.

Elevated Level – Elevated periods are defined to be slightly elevated and not associated with macroscopic flaring events.

$$2.5 \times R_{char} + 1.5\sigma > R_{block} > 1.2 \times R_{char} + 1.5\sigma \tag{2}$$

In the middle panel of Figure 2 there are nine such blocks, only one of which is not associated with a flare.

Very Elevated Level – The remaining blocks are defined as very elevated periods:

$$R_{block} > 2.5 \times R_{char} + 1.5\sigma \quad (3)$$

These are intense enough that they are often associated with macroscopic flaring events. In Figure 2, there are five such blocks.

Flaring – The key to identifying a flare by eye within a “very elevated” period is its rapid flux change. Hence, it is natural to add the derivative of the lightcurve (dR/dt) (or the second derivative of the photon arrival time) to the criteria. The difference between successive block rates can easily be chosen as dR , but defining dt requires careful thought. A simple definition of dt as the interval between the mid-time of consecutive blocks would dilute truly rapid rises, especially when observation gaps exist. We instead choose dt as the shorter of the exposure times in two successive blocks. To prevent a dependence on rate, dR/dt is scaled by the inverse of R_{char} . By plotting $1/R_{char} \times dR/dt$ and the lightcurve simultaneously we empirically determined a threshold of $1/R_{char} \times dR/dt > 10^{-4} \text{ s}^{-1}$ to be indicative of a flare. A flare is defined as a successive series of elevated blocks which include at least one very elevated block and one period in which

$$1/R_{char} \times dR/dt > 10^{-4} \text{ s}^{-1} \quad (4)$$

In the bottom panel of Figure 2, we plot 24 values of:

$$\Delta = 1/R_{char} \times dR/dt \quad (5)$$

Ten of these exceed our threshold, and seven are associated with very elevated levels. Grouping the consecutive occurrences, we find three flares. The blue lines in the third panel of Figure 2 and the similar panels of Figure 3 identify the full durations of the flares.

A weakness of this set of definitions is the rather stringent requirement of flare strength. Only intervals for which the stellar luminosity rises by more than a factor 2.5σ above 120% of the characteristic level are definable as flares. In practice, the smallest luminosity change associated with a flare is a luminosity change of a factor of three. Flares moderately weaker than this are relegated to the “elevated” category. Any activity that increases the overall flux by less than $\sim 50\%$ is completely ignored and accounted for in the characteristic data.

The levels chosen for our definitions are admittedly subjective – especially the factors 1.2 and 2.5σ that enter in the definition of elevated vs. characteristic levels and the setting

of the flare level Δ at $1/R_{char} \times dR/dt > 10^{-4} \text{ s}^{-1}$. These definitions are tuned to match what we intuitively agree are significant flares. Some probable flares are missed, such as the second very elevated period for COUP 1134.² Some marginal events are also counted such as flares, e.g., the final three flares on COUP 314, where a low characteristic rate serves to exaggerate the rate of change. In testing several variations on these numbers to arrive at our final criteria, we found that some weaker flares are lost and others are found. Based on this experimentation, we estimate that the total number of flares is reliable at the $\pm 10\%$ level with respect to variations in the criteria of equations (1)–(4).

Figure 3, shows the lightcurves for the 28 solar mass sources in the ONC. The lightcurves are presented as histograms with blocks of constant flux overlaid. A new block is used when maximum likelihood statistics indicate 95% confidence that the data are not consistent with a constant signal. The lower plot in each panel indicates $1/R_{char} \times dR/dt$ between each pair of blocks. Flares are indicated with lines above the lightcurves.

4. Spectral Fitting

Much of the analysis of pre-main sequence flaring in this study will be based on spectral modeling of the COUP source spectra in terms of optically-thin plasmas in collisional equilibrium. From this modeling we extract plasma temperatures, instantaneous luminosities and time-integrated energy output in the *Chandra* 0.5 – 8 keV band. We assume elemental abundances follow the cosmic abundance pattern with 0.3 times the solar abundance. This may be a poor assumption as abundance anomalies and temporal variations have been seen in other magnetically active stars (e.g., Favata & Schmitt 1999, Brinkman et al. 2001) and are present in some COUP sources (G05). Abundance effects will be treated in a later COUP study, but their omission here should have little effect on our determinations of broad-band luminosities and energies.

We employ the usual corrections as discussed in G05 to fit the spectra of the photons which arrived during characteristic periods to a two-temperature MeKaL plasma. MeKaL was used as a convention by the COUP team. We found that if N_H is left as a free parameter, there is a strong correlation between luminosity and N_H (luminosity increasing with increasing N_H). This is due to a natural degeneracy in the problem: one can arrive at a uniformly good fit by increasing N_H and the high temperature flux in parallel.³ For this

²Since it is seen just coming out of a perigee passage, its rise time is seriously overestimated and its slow decay prevents detection of a rapid decline.

³This degeneracy is exacerbated when using the front illuminated CCDs of ACIS-I since they have low

reason, N_{H} was frozen at $A_v \times 1.6 \times 10^{21}$. An exception was made when the fit was formally poor; when $\chi^2/d.o.f > 2.5$, we allowed N_{H} to become a free parameter.

Once the characteristic spectra are determined, we proceed with the remaining spectral analysis of each star. All photons that arrive during elevated periods are combined into a composite elevated spectrum for each star. Photons that arrive during flare periods are separated to create spectra for each flare. Except where noted, each of these ~ 70 spectra is fit by a one or two-temperature MeKaL plasma with N_{H} and metallicity frozen to the characteristic values. We show an example of this fitting process for COUP 262 in Figure 4. In practice, four stars⁴ needed N_{H} to become a free parameter regardless of whether characteristic, elevated or flare data were being fit. This could be due to high local extinction, to unusually high coronal temperatures, to a broad range of coronal temperatures or to poor extinction estimates. Data for these stars should be treated cautiously. In addition, no spectral fits were performed for COUP 828 in flare because its proximity to a chip gap confused our flare detection algorithm.

5. Analysis

In this section, we examine the sources in the three states, characteristic, elevated and flare. We compare the luminosity and plasma temperatures in these states. We focus characteristics which will have the greatest effect on matter near the star, including the peak luminosity and temperature, as well as the frequency and duration of flares.

5.1. The Characteristic Level

Table 4 shows the results of the spectral fits for each star’s characteristic level. The first column indicates the COUP source ID, the second gives the interval the source spent at the characteristic level. Columns 3–5 give the number of bins, the χ^2 per degree of freedom and the null probability. Columns 6–11 give N_{H} (converted from A_V or fit), the temperatures of the cool and hot coronal components, ratios of the emission measures of the cool to hot component, the resultant luminosity assuming a distance of 450 pc and the energy released between 500 eV and 8 keV during the indicated interval. The final column notes where N_{H} was allowed to be a free parameter.

effective area at low energy where the absorption is most important.

⁴COUP 241, 250, 262 and 314.

On average, sources were at their characteristic levels for about 640 ks out of 850 ks or 75% of the time.⁵ Restricting our sample to sources with high-quality (i.e., acceptable χ^2) two-temperature fits, the median luminosity of the characteristic level is $\log L_t = 30.25$ ergs s^{-1} . The dashed line in Figure 5 shows the distribution of these characteristic luminosities. This is consistent with the results from Flaccomio et al. (2003) who found a median luminosity of $\log L_t \sim 30.5$ ergs s^{-1} for stars between 1 and 2 M_\odot and $\log L_t \sim 30.05$ ergs s^{-1} for stars between 0.5 and 1 M_\odot . Their use of a “basal flux” (similar to our characteristic flux) mitigated bias due to large flares that occurred on about 5-10% of the stars in their sample. Our result is slightly lower than the average luminosity found for solar mass stars by FGP02. The characteristic $\log L_{t,c}$ is roughly uniformly distributed with a MAD of about half a dex (0.49).

We expected to find L_{char} and bolometric luminosity to be well correlated since the flaring component has been removed from the determination of X-ray luminosity. Indeed, both Spearman (τ) and Kendall (ρ) correlation coefficients show greater than 99.98% confidence in the correlation. A two-variable linear regression first order fit finds $\log L_{char} \propto \log L_{bol}$ such that $\log L_{char}/\log L_{bol} \simeq -3.58$ with $MAD = 0.21$. In these data, we focus solely on the characteristic X-ray flux from the star. In summary, about 0.03% of a star’s luminosity is characteristically released as X-rays between 500 eV and 8 KeV.

We also examined the relation between characteristic luminosity and age. We find $\rho = 0.12$, a weaker correlation than that reported by FGP02 and consistent with no correlation. As shown in Figure 6, we fit the data to an outlier-resistant two-variable linear regression giving $\log L_{char} = 32.1 - 0.47\log(t)$, where t is in units of a million years. The 1σ scatter from this fit is 0.35 in units of $\log L_{t,c}$. This is a flatter relationship than that reported by FGP02 who found a slope of $1.1\log(t)$. Our slower evolution within the COUP age range was also found in the COUP study of Preibisch & Feigelson (2005).

5.2. Elevated and Very Elevated Levels

FGP02 used “a simple subjective classification of the variations” observed in solar mass stars. They classified stars as constant, long term variable, possible flare and flare. They found ~ 30 flares or possible flares on 43 stars (69%) in 50 ks of observing time. At that rate, we should see ~ 12 flares per star or about 350 total flares, and in fact, this is very

⁵This is in remarkable agreement with Osten et al. (2004). Over a four year coordinated campaign, they found that the RS CVn System HR 1099 has a 30% duty cycle for coherent low frequency radio emission. The flare frequency cited by Osten & Brown (1999) is somewhat higher ($\sim 40\%$).

close to our total number of MLBs. Using our definitions, we find ~ 40 flares on 28 stars in about 17 times the observing time of the FGP02 data. In this sense, our definition is about a factor 10 times more conservative than that of FGP02. We have instead termed these ~ 300 “missing” flares as “elevated” level intervals; this activity is not “missed”, it is merely accounted differently. Since we are concerned with the effect on the protoplanetary disks, the relevant quantities are the duration, luminosity and temperature of X-rays during elevated periods.

Table 5 shows the results of the spectral fits to data from each star’s periods of elevated flux. The column definitions are the same as those for Table 4. The median duration in the elevated regime is about 65 ks out of the total 850 ks; i.e., on average, sources are elevated only about 8% of the time. This is consistent with the definition that the flux is between 1.5 and 2.5σ above the characteristic level, and luminosity changes are similarly limited to be between 1.6 and 2.6 times the characteristic luminosity. There is evidence that the periods of elevated flux are indeed associated with microflaring as the median temperature of the hot component of the corona goes up by 25% during these periods - from a median of 2.34 keV (MAD = 0.7) to a median of 2.93 keV (MAD = 0.7) - while the cool component stays constant.

There are only 6 periods of very elevated rates that failed to start with a rapid rise of $\Delta > 10^{-4}$ and were therefore not classified as flares. The duration of non-flaring yet very elevated fluxes represents only 1.2% of the total observing time. The very elevated periods are associated with modest luminosity changes of between 2.5 and 5. The median temperature of the hot component of the corona goes up further to about 3.1 keV while the temperature of the cool component stays constant at around 800 eV.

5.3. Flaring

5.3.1. Strength and Duration of Flares

Forty-one flares were detected at 95% confidence.⁶ There is no single objective method for determining the duration of a flare, but there are two obvious extremes: concentrating just on the temporal region of the peak of the flare or considering the entire time that the count

⁶Using maximum likelihood statistics, blocks are formed on the basis of confidence that the data are not consistent with constant and hence a new block is needed. The determination of a flare follows equations (1)-(4). The determination of the duration and the rates of the blocks are subject to the confidence in that block.

rate is elevated. In adapting the latter “whole flare” approach, we looked at “prototypical” flares like that of COUP 262 or the two flares on COUP 223. In these cases, the tail of the flare includes both “elevated” and “very elevated” blocks. Here we could define the duration of a flare as the total duration of all successive elevated blocks adjacent to a flare. The range of flare durations is vast, from 1 hr to 3 days as shown in Figure 7.

Table 6 contains the spectral fits to all the flares with at least 50 photons to fit. The columns in this table are identical to the two previous tables except that the results for each flare are tabulated separately. The luminosities and temperatures represent averages of each flare whereas the energy gives the total released in the event. The median $\log L_{t,c}$ was about $30.81 \text{ ergs s}^{-1}$ with the median temperature of the hot coronae of about 3.45 keV. The cool corona remained near 800 eV. The ratios of flare to characteristic luminosities, plotted in Figure 8, show that most flare amplitudes are not extremely high. The median flare level is 3.5 times the characteristic level, and 90% of flares rise to less than 10 times the characteristic level.

The luminosities of the peak blocks are another measure of flare intensity. Table 7 lists the spectral fits to just the peak of each flare (if there were enough photons to yield a reliable fit). As can be inferred from Figure 5, the peak flare luminosities are about 0.25 dex higher than the integrated flare luminosities (median $\log L_{t,c}/\log L_{bol} = -2.77$). This method of calculation has little effect on the relative strength deduced for each flare, the median ratio of the peak to characteristic luminosity is 6. The largest change was observed during the second flare of COUP 1259, when the ratio of the peak to characteristic luminosity soared to 80. The median peak $\log L_{t,c}$, was about $30.97 \text{ ergs s}^{-1}$, while the median duration of peak blocks is about 10 ks. More importantly, the median plasma temperature was about 7 keV during the peak of each flare! The most luminous period is also likely the hottest portion of the flare and is therefore the most capable of affecting circumstellar material.

There are no strong trends of the duration of flares relating to the luminosity. Specifically we find no direct relation between flare duration and either peak intensity or average luminosity. The ρ rank correlations were 0.88 and 0.41 respectively – consistent with no correlation. We find a median “whole flare” duration of about 65 ks or about 6.5 time longer than the period of peak intensity.

5.3.2. Energy Release in Flares

Having determined the duration and the luminosity of each flare we can now discuss the energy released during each event. Multiplying the full duration of each flare by its

luminosity (columns 3 and 11 of Table 6) we calculated the total energy released during the event (column 12): The median flare released about $10^{35.5}$ ergs. Most energetic, was the second flare on COUP 1259 which was an order of magnitude brighter than any other. Figure 9 shows the cumulative number of flares for a given energy. Fitting the data below 10^{36} ergs demonstrates that the number of flares releasing a certain energy can be expressed as $N = 1.1 \log E^{-0.66}$. Differentiating the equation solves for the number of flares as a function of energy: $dN/dE \propto E^\alpha$ with $\alpha \simeq 1.7$. The largest uncertainties in the fit are not statistical, but rather come from the fitted range. Constraining the fit to energies below 10^{35} ergs the power law index is decreased by 0.11 to $\alpha = 1.55$.

Measurements of the X-ray flare energy distribution index lie in the range $1.5 < \alpha < 2.5$ for the Sun and $1.5 < \alpha < 2.7$ for magnetically active stars (Güdel et al. 2003). A key difference for the Sun is that the total energy released in a flare is less than 10^{32} ergs (cf. Figure 6 in Crosby, Aschwanden & Dennis 1993). Several groups (Collura et al. 1988, Pallavicini, Tagliaferri, & Stella 1990) derived $\alpha = 1.5$ -1.7 for a sample of M-dwarf flare observations with EXOSAT. Our result is also consistent with distribution of X-ray flares on the contemporary sun and other active stars reported by earlier authors $dN/dE \propto E^{-1.7 \pm 0.1}$ (Hudson 1991, Crosby, Aschwanden & Dennis 1993). Recent statistical investigations suggest $\alpha = 2.0$ -2.6 for small flares in the quiet solar corona (Krucker & Benz 1998; Parnell & Jupp 2000).

Our flare distribution is cut off below 10^{34} ergs which arises from the classification criteria that require the flares to lie ≥ 3 times above the characteristic luminosities around $\log L_t \simeq 30.5$ ergs s^{-1} . The overall lightcurves are not consistent with all the X-rays being produced by a single power law extending down to zero counts. The overall appearance of the lightcurves is a relatively constant characteristic level with sudden big flares. Inspection does not show obvious low frequency signal which would be expected due to the superposition of intermediate and low-intensity flares as implied by a power law.

To demonstrate this in a qualitative manner with a simple simulation. We created a simulated 13.2 day lightcurve with a “toy” template flare (rapid rise, 10-hr exponential decay and a distribution following a power law. The main free parameter was dN/dC , where C is the number of counts in a flare (modeling the energy is beyond the scope of this study). Simulations were performed with $dN/dC \propto C^{-1.7}$, $dN/dC \propto C^{-2}$, $dN/dC \propto C^{-2.5}$ and $dN/dC \propto C^{-3}$, and created lightcurves by the superposition of flares. To compare results for high and low count rate sources, the number of flares was varied from 100 to 4400. For each power law index 100 simulations were run at each flare quantity.

Some examples of our 43,000 simulations are shown in Figure 10. By inspection, it appears that if all of the X-rays are produced by flaring and if the flares follow a single

power law, values of the power law index of -1.7 would create more flares than are seen in our data. Similarly, the power law index of -3 produces too few flares. If the sole source of the X-rays were flaring drawn on a single power law, the index would have to be about -2.25, which is too steep to describe the brightest flares. Thus, either flare energies are better represented by a broken power law, or by a single power law overlying an X-ray continuum. Güdel et al. (2003) recently reported on EUVE and BeppoSAX observation of the nearby dMe star AD Leo, ascribing all the activity to small-scale flaring with α values between 2.0 and 2.5. A full quantitative comparison with the whole COUP dataset is beyond the scope of this paper and would require more extensive work over a broad range of masses.

The total energy release in each flare is nearly linearly correlated with the luminosity. The best fit to a linear regression is

$$Energy \propto Luminosity^{1.16} \quad (6)$$

The MAD of the fit is 0.38 dex and the rank correlation is correspondingly strong ($< 10^{-5}$). Since energy and luminosity are linearly related i.e. $Energy = Luminosity \times Duration$, it follows that the duration is essentially independent of the luminosity of the event. As far as can be determined from this sample moreover, the energy and luminosity of flares are independent of age.

5.3.3. Frequency of Flares

We found 41 large flares during an average effective exposure time of 660 ks on 27 observed solar mass stars (COUP 828 was excluded from flare searches because of its proximity to a chip gap). Thus, we compute a preliminary average of 1 flare per star per ~ 435 ks of observing time. The true rate of flares is somewhat lower than this; however, because the effective exposure time on some sources was limited due to dither and off-axis effects. While such effects lower the total number of counts observed, the overall sensitivity to flares is not compromised because all flares observed exceed the duration of the dither cycle. We argue that we are sensitive to flares that occurred on any of the 27 stars during the full 850ks observation. Further, flares which occurred when the ONC was not being observed would still have been detected as such if the flare lasted into the next observing window. Although we cannot detect any flares that take place entirely during perigee passage by *Chandra*, we do detect flares that begin during the perigee passage and extend to about 8 hours after perigee, when new observations start. Since the median flare duration is about the same length as perigee passage, we miss about half of the flares that begin during perigee. The time between observations is about 57 ks, and there were five perigee passages during the observations, so

we were sensitive to one half of the flares occurring during about 288 kiloseconds of perigee passages. Applying these corrections, we infer an average of 1 flare per star per 650 ks. This is consistent with earlier results for Orion and much older clusters as reported by Wolk et al. (2004). However the flare definitions used were less quantitative than those used here and biases in the data are unclear. Specifically, Wolk et al. (2004) were more sensitive to faint flares that would be considered elevated in the current work. Nonetheless, it appears that flare rates change by a factor less than 5 during the first 100 Myrs.

Two stars, COUP 1023 and 1281, show no evidence of flaring. COUP 241, 1167 and 1159 only showed flaring in the extremely early or late observation intervals. Eleven stars underwent two flares, one star was observed to have three, and another exhibited four. *A priori* we did not consider the quiet nature of COUP 1023 and 1281, or the active nature of COUP 314 and 567, anything more than statistical fluctuation in a random distribution of flares. On the Sun however, the observed power-law distribution of flare energy release is well characterized by the assumption that the solar corona is critically self-organized (Lu & Hamilton 1991). A result of this organization is a waiting time distribution (Lu et al. 1993) between flares that is power law in nature with a slope of $f(t) \propto t^{-\Gamma}$ where the index Γ is about 2.15-2.55 (Wheatland 2000, Norman et al. 2001).

To test whether stars in the sample were subject to a nonrandom waiting time, we assumed that all stars in the sample have the same behavior (and thus that observing 27 of them for 850 ks is equivalent to observing one of them for 24 Ms – the ergodic theorem). The distribution was simulated using a simple Monte Carlo model for the distribution of flares among the 27 stars. For each star, the lightcurve was divided into 39 25 ks bins, assigned a random number to each bin, if the random number exceeded a threshold, we noted this as a flare. We set the threshold to trigger once per 625 ks (25 bins) on average. One thousand datasets of 27 stars were simulated, each with about 41 flares in each dataset. The results of the simulation are shown in Figure 11. Not surprisingly, the result is a Poisson distribution centered between 1 and 2 flares per star with a few extra sources in the zero flare bin since it is impossible to have negative flares. A two-sided KS test fails to discriminate the ergodic model from other models (probability that the data fit the ergodic hypothesis was 44%). Thus, at the level of our data, there is no indication that the temporal distribution of flaring is anything other than random.

5.3.4. *Shape of Flares*

In our initial qualitative analysis of the bright flares in the dataset, we categorized flares by luminosity, duration and shape. Specifically, the shape was noted as either, “linear rise

plus exponential decay”, “symmetric” or “spike” (i.e., less than 5 ks from beginning to end). There were also a handful of flares which were too weak to describe. Eight flares were noted as symmetric. The first flare of COUP 1259 is probably the best example of a slow-rise roughly symmetrical flare. In two sources, COUP 131 and 1570, multiple symmetric events may be indicative of rotational modulation of long-lived structures in the stellar corona, rather than individual magnetic reconnection events (these are detailed by Flaccomio et al. 2005). Three of the remaining five symmetric events are too short-lived to be rotational events (durations <1 d) and are not seen to repeat.

5.4. Temperature

The temperature profile of the flares is critical to understanding their ability to penetrate circumstellar material. Harder X-rays penetrate more material and can heat deeper into disks’ midplanes. A fundamental question is whether or not the flare plasmas of these T Tauri stars share properties known in flare plasmas of older stars, including: $L_x \propto kT_1^{2.2}$ (Preibisch 1997), $L_x \propto kT_2^5$ (Güedel et al. 1997) and kT_1 is always around 0.8 keV (Sanz-Forcada et al. 2003) where T_1 and T_2 are the cooler and hotter plasma components, respectively.

We have fit most of the X-ray sources as two temperature MEKAL models. We find a significant correlation between the hot and cool components of the characteristic X-ray emission as shown in Figure 12. A similar effect was seen in ROSAT data albeit with a different instrument and for different stars (cf. Stern et al. 1994, Gagné et al. 1995 and Figure 24 of Favata & Micela 2003). The effect has also been noted in the time-integrated spectra of COUP stars (Preibisch et al. 2005a).

At the characteristic levels, the soft component is weakly correlated with the characteristic luminosity (correlation coefficients indicate < 0.15 probability of no correlation) and the harder component shows no correlation whatsoever ($\tau; \rho; \sim 0.90$). However, the characteristic hot and cool coronal components are highly correlated: a linear regression fit gives $kT_2 = 2.14 \times kT_1 + 0.66$ keV, with a median deviation of 0.5keV about the fit. A key difference between this data set and the ROSAT results mentioned above is the hard sensitivity and corresponding lack of soft X-ray sensitivity of the Chandra ACIS-I. Thus, it is not surprising that we find a hard component median of about 2.3 keV and a median soft component around 0.9 keV, both much warmer than found with ROSAT.

The temperature correlation breaks down during the elevated and flare periods ($\tau, \rho \sim 0.25$ for both flare and elevated periods). It is clear that the temperature of the hot component of the plasma increases as a star’s flux level changes from the characteristic level to the

flaring state; the hot plasma achieves maximum heating when the star is at peak flux levels. The cool components do not change significantly. This evidence suggests that the breakdown in the correlation occurs because the flare is only manifest in the hot corona. The median of the hot component increases by over 50% to 3.45 keV during flares, and five flares exceeded temperatures of 100 MK (9 keV) in their hot component. Favata et al. (2005) examined the brightest flares in the COUP sample and found 100MK temperatures in half of the events. This is supporting evidence for a L_x - kT_2 relationship. Further, it implies that hotter flares than those witnessed during this 13.2 day observation probably occur on these stars. The cool component shift (formally from 670 eV to 760 eV) is consistent with a constant kT_1 as found by by Sanz-Forcada et al. (2003).

5.5. Stars With and Without Disks

We have reasonable disk and flare data on 26 of the 28 stars in the sample but lack $\Delta(I - K)$ measurements for two stars (Table 2). Three stars have evidence of accreting disks via Ca II emission lines, while 13 have evidence of passive accretion disks as ascertained by a K band excess or direct proplyd detection without Ca II emission lines. Ten stars have no evidence of a disk. Among the active accretors, two are faint with a single weak flare, and one, COUP 567, has multiple strong flares. The group of stars with passive accretion disks include the two obvious rotators: the star with four flares and another star with no flares. The subgroup without evidence of any disk also contained one star without flares and its remaining stars had one or two modest flares. There is thus no evidence dependence of flare properties on the presence of dusty disks or accretion. This issue will be revisited in a future COUP paper using larger samples.

6. X-ray Interactions with Circumstellar Disks

As is the case for all YSOs, X-rays from the Sun-like stars in the ONC affect conditions in their immediate environment (see e.g., the review by GFM00). In a dense cluster, nearby stars may contribute, but close to any given star, the X-ray emission from that star (and any companion) will dominate. Having found that solar mass stars have a characteristic X-ray luminosity, it is appropriate to update the formula given by GFM00 for the ionization rate ζ at a radial distance r (in units of AU) from a YSO (see also Glassgold, Najita, & Igea 2004),

$$\zeta = 6 \times 10^{-9} \text{ s}^{-1} \left(\frac{2 \times 10^{30}}{L_{char} [\text{ergs s}^{-1}]} \right) \left(\frac{\text{AU}}{r} \right)^2. \quad (7)$$

This formula ignores likely attenuation and scattering of the X-rays, and uses the median characteristic X-ray luminosity given in §6.1, which is appropriate for solar mass stars; this value is lower for more common lower mass stars.

In their calculation of the production of short-lived radionuclides in the region near and inside the inner disk or co-rotation radius, Lee et al. (1998) invoked observations of soft and hard YSO X-rays made with ROSAT and ASCA to estimate the fluence of nuclear particles. They converted X-ray to stellar energetic-particle fluxes using observations of the contemporary active Sun. A related calculation by FGP02 using *Chandra* observations estimated that the particle fluxes from active YSOs were $\sim 10^5$ more intense than in the active Sun. This number reflects the fact that YSO flares are more powerful and more frequent than those of the contemporary Sun, and that the energy distribution of solar energetic particles is shallower than that for X-rays. FGP02 found that the inferred increase of 10^5 in particle fluence is more than sufficient to explain by spallation the abundances of several important meteoritic isotopic anomalies (Woolum & Hohenberg 1993, Lee et al. 1998, Goswami et al. 2001, Gounelle et al. 2001, Marhas et al. 2002, Leya et al. 2003).

Our COUP observations of solar-mass YSOs can be used to make similar estimates of the particle fluence in the reconnection ring. If we take the mean characteristic luminosity as 2×10^{30} ergs s $^{-1}$, and the mean flare luminosity, duration, and repetition times as 6×10^{30} ergs s $^{-1}$, 10^5 s, and 650 ks respectively, the fluence at a distance $0.75R_x$ (with $R_x = 0.05$ AU, the x-point or co-rotation radius) over 10 years becomes:

$$\mathcal{F}_X(10 \text{ yr}) = 2 \times 10^{15} \text{ ergs cm}^{-2}. \quad (8)$$

If we now convert from X-ray to proton fluence (for energies greater than 10 MeV) using the same 0.1 factor as used by Lee et al. (1998), we get essentially the identical result as those authors,

$$\mathcal{F}_p(10 \text{ yr}) = 2 \times 10^{14} \text{ ergs cm}^{-2}. \quad (9)$$

Individual stars will exhibit a scatter of a factor of ± 3 or more about these values. A caveat to be discussed further in the next paragraphs is that the nuclear irradiation of calcium-aluminum inclusions (CAIs) probably occurred at an earlier stage of pre-main sequence evolution than seen in the unobscured ONC stars considered here.

A potentially important connection permitted by the COUP's 13.2-day exposure is that very short ($\lesssim 1$ hr) as well as long duration ($\gtrsim 1$ d) flares observed are reminiscent of solar impulsive and gradual flares. Although the COUP data cannot directly detect the brief very-hard spectral signature of impulsive phases at the beginning of ONC flares, we can infer by analogy with the relationship of solar impulsive and gradual flares that the impulsive phase is often present. This may be very significant since, on the contemporary Sun, impulsive and

gradual phases of solar flares have different properties, most strikingly in their elemental and isotopic composition. Unlike proton-rich gradual events, which are also associated with coronal mass ejections, impulsive events are ^3He rich, and are therefore particularly effective in producing some short-lived radionuclides like ^{26}Al and ^{41}Ca , but not ^{60}Fe . (Lee et al. 1998, Gounelle et al. 2001).

As basic as the nuclear fluence estimates are, the YSO X-rays can also directly affect the physical state of the irradiated material, i.e., the proto-CAIs and chondrules seen in the earliest solar system solids. Favata et al. (2005) examined two of the stars in our sample COUP 223 and COUP 262 and fit these events to coronal loop models. They find that the flare in COUP 262 extended at least $3.6R_*$ and may have reached $18R_*$ indicating possible direct contact between the inner portion of the disk and magnetic loop of the flare. According to Lee et al. (1998) and Gounelle et al. (2002), solids experienced thermal processing episodes for several years before being launched into the primitive solar nebula. These events induced a variety of phase changes, including partial or full evaporation. Shock waves from these powerful flares may also propagate along the outer layers of the protoplanetary disk and melt proto-chondrules several A.U. from the star (Nakamoto et al. 2005). Powerful flares, such as those at the high end of the distributions in Figures 5, 8 and 9, may thus have important effects on the solar nebula disk material in several ways. Their hard penetrating X-rays will ionize disk gas, even into the midplane. Their energetic baryonic particles may produce short-lived radionuclides in disk solids via spallation with their energetic particles. Their thermal flashes or shock waves may melt disk dustballs into CAIs or chondrules.

This particular application also points out an important limitation of the *Chandra* observations that will be difficult to overcome without a significant enhancement in the capability of X-ray observations. Most of the YSOs observed in the ONC, including the solar-analog sample of this paper, are revealed T Tauri stars with a median age of the order of 2 Myr. Although a fair fraction have disks and are still accreting, most of the stellar mass has already been accreted, following an earlier more active stage of accretion that probably occurred during the first several hundred thousand years of their lives. It is very likely that the nuclear irradiation that led to some, if not many, of the short-lived radionuclides occurred during this early period and not in the T Tauri phase. We note that the meteoritic evidence for high energy processes that we attribute to X-ray flares takes place over an extended and complex period. CAIs are irradiated and melted during a brief ($< 10^4$ yr) protostellar phase, chondrules are melted over a somewhat longer phase (10^5 yr), while grains showing spallogenic ^{21}Ne excesses are irradiated over 10^7 years. Although the sample of young solar analogs studied here was selected to be unobscured $\sim 10^6$ year old stars, we note that both the younger COUP stars embedded in the OMC-1 cloud cores (Grosso et al. 2005) and older COUP stars ($\simeq 10^7$ yr; Preibisch & Feigelson 2005) exhibit very similar X-ray luminosity

functions and flaring behavior as the sample examined here. It is perhaps uncertain only whether or not X-ray emission extends to the very youngest Class 0 protostars.

7. Summary and Conclusions

We have examined a sample of 28 solar–mass stars observed by *Chandra* during a very deep observation and have quantified the lightcurves of the X-ray sources using maximum likelihood analysis. Taking advantage of the extremely long and nearly continuous nature of the observation we applied quantifiable definitions to the lightcurves to identify characteristic levels, flares and intermediate states for 27 of these sources. Principle among our findings is that young solar analogs spend about three-fourths of their time in a relatively well behaved characteristic state. This state can be well modeled as a 2–temperature plasma with one component fixed near 850 eV and the other component of about 2.35 keV. This characteristic state is marked by good correlations among their coronal temperatures and bolometric to X-ray luminosities, but these relationships break down in the more active states. While the flares are well fit by $dN/dE \propto E^{-1.7}$, a power law index of ~ -2.25 is required to match the shape of the overall lightcurves if they are purely the result of flaring. This broken power law is consistent with recent observation of RS CVn stars (for bright flares) and AD Leo (for fainter flares) and indicates that the characteristic portion of the luminosity does not arise from flares (or at least not the same kind of flares that give rise to the luminosity in the flaring state). The emission of the stable component represents about 0.03% of the bolometric luminosity.

Some of our conclusions regarding behavior during the very complex flaring state are as follows:

1. The median flare has a luminosity of about $10^{30.8} \text{ergs s}^{-1}$ and releases about $10^{35.5}$ ergs with $kT_{hot} \sim 3.45$ keV. The peak luminosity of flares is almost $10^{31} \text{ergs s}^{-1}$ and lasts about 10ks. During the peak of the flare kT_{hot} has a median of about 7 keV.
2. The ratio of the flare peak to characteristic flux is less than a factor of 100. Flares induce a large change in the temperature of the hot coronal plasma component.
3. We find no relation between luminosity and duration, nor do we see significant trends of luminosity with age.
4. There is no statistical evidence that flares are subject to a waiting time between flares. The time between events can be modeled as a random occurrence. The duration of the flares themselves varied from less than an hour to almost three days.

5. The cool component of the corona is unaffected by activity, with the median value of kT_{cool} remaining between 710 and 900 eV in all states.

The intensity and hard spectra found for ONC solar analogs indicate that the resulting ionization of disk gases by stellar X-rays dominates ionization by cosmic rays or other sources by a large factor. If solar-type particle production is associated with thermal flares, the observed flaring rate inferred for the early Sun is sufficient to produce many of the isotopic anomalies seen in meteoritic inclusions.

X-rays do not account for all anomalies seen in meteoritic inclusions or protosolar analogs. Although X-ray heating of gas above the midplane is significant and rotation–vibration transition of CO should be easily excited. But this does not occur at rates significant enough to explain recent observations of very strong CO signature in some T Tauri stars.

We thank the referee Alex Brown for a critical reading and helpful suggestions regarding all aspects of the manuscript. We are extremely grateful to A. Glassgold for helping to lay out the arguments in the second to last section and several critical readings. We thank Salvatore Sciortino (Palermo) for a critical reading of this paper and Jay Bookbinder (SAO) for a valuable discussion. This research made use of SAOImage DS9, developed by the Smithsonian Astrophysical Observatory. This research also made use of the Two Micron All Sky Survey (2MASS), a joint project of the University of Massachusetts and the Infrared Processing and Analysis Center/California Institute of Technology, funded by the National Aeronautics and Space Administration and the National Science Foundation. COUP is supported by Chandra Guest Observer grant GO3-4009A (E. Feigelson, PI). S.J.W. and F.R.H. received support from *Chandra* X-ray Center contract NAS8-39073 and HRC contract NAS8-38248, E.D.F. received support from *Chandra* ACIS contract NAS8-38252, E.F, G.M. and S.S. received support from the *Ministero dell’Istruzione dell’Università e della Ricerca*.

Facility: CXO(ACIS) 17, 54, 57, 131, 147, 177, 223, 241, 250, 262, 314, 515, 567, 753, 828, 1023, 1127, 1134, 1151, 1167, 1235, 1259, 1281, 1326, 1327, 1500, 1539, 1570

REFERENCES

- Balbus, S. & Hawley, J. F. 1991, ApJ, 376, 214
- Bary, J. S., Weintraub, D. A., & Kastner, J. H. 2003, ApJ, 586, 1136

- Bower, G. C., Plambeck, R. L., Bolatto, A., McCrady, N., Graham, J. R., de Pater, I., Liu, M. C., & Baganoff, F. K. 2003, *ApJ*, 598, 1140
- Brinkman, A. C., et al. 2001, *A&A*, 365, L324
- Collura, A., Pasquini, L., & Schmitt, J. H. M. M. 1988, *A&A*, 205, 197
- Crosby, N., Aschwanden, M., & Dennis, B. 1993, *Advances in Space Research*, 13, 179
- D’Antona, F., & Mazzitelli, I. 1994, *ApJS*, 90, 467
- D’Antona, F. & Mazzitelli, I. 1997, *Mem. Soc. Astro. Ital.*, 68, 807 [DM97]
- D’Alessio, P., Calvet, N., Hartmann, L., Lizano, S. & Cantó, J., 1999, *ApJ*, 527, 893
- Dennis, B. R. 1988, *Sol. Phys.*, 118, 49
- Desch, S. 2004, *ApJ*, 608, 509
- Dorren, J. D., Güdel, M., & Guinan, E. F. 1995, *ApJ*, 448, 431
- Favata, F. & Micela, G. 2003, *Space Science Reviews*, 108, 577
- Favata, F., & Schmitt, J. H. M. M. 1999, *A&A*, 350, 900
- Feigelson, E. D. & Decampli, W. M. 1981, *ApJ*, 243, L89
- Feigelson, E. D., & Montmerle, T. 1999, *ARA&A*, 37, 363
- Feigelson, E. D. 1982, *Icarus*, 51, 155
- Feigelson, E. D., in *Cool Stars, Stellar Systems and the Sun 13*, F. Favata & J. Schmitt, eds., (Noordwijk: ESA SP), in press
- Feigelson, E. D., Garmire, G. P., & Pravdo, S. H. 2002, *ApJ*, 572, 335 [FGP02]
- Flaccomio, E., Damiani, F., Micela, G., Sciortino, S., Harnden, F. R., Murray, S. S., & Wolk, S. J. 2003, *ApJ*, 582, 398
- Flaccomio, E. Micela, G. et al. (2005) *ApJS*, this issue (COUP rotation paper)
- Flaccomio, E., Micela, G., & Sciortino, S. 2003, *A&A*, 397, 611
- Güdel, M., Guinan, E. F., & Skinner, S. L. 1997, *ApJ*, 483, 947
- Gagné, M., Caillault, J., & Stauffer, J. R. 1995, *ApJ*, 445, 280

- Gammie, C. F. 1996, *ApJ*, 457, 355
- Garay, G., Moran, J. M., & Reid, M. J. 1987, *ApJ*, 314, 535
- Getman, K. V., et al., 2005, *ApJS*, this issue [G05] (COUP obs/sources paper)
- Glassgold, A. E., Feigelson, E. D., Montmerle, T., & Wolk, S, 2005, in *Chondrites and the Protoplanetary Disk*, A. Krot et al. eds., (San Francisco: ASP) in press
- Glassgold, A. E., Feigelson, E. D., & Montmerle, T. 2000, in *Protostars and Planets IV*, eds V. Mannings et al., (Tucson: Univ. Arizona Press), 429
- Glassgold, A. E., Najita, J., & Igea, J. 2004, *ApJ*, 615, 972
- Glassgold, A. E., Najita, J., & Igea, J. 1997, *ApJ*, 480, 344 [Errata: *ApJ*, 485, 820, 1997]
- Goswami, J. N., & Vanhala, H. A. T. 2000, in *Protostars and Planets IV*, eds V. Mannings et al., (Tucson: Univ. Arizona Press), 963
- Goswami, J. N., Marhas, K. K., & Sahijpal, S. 2001, *ApJ*, 549, 1151
- Gounelle, M., Shu, F. H., Shang, H., Glassgold, A. E., Rehm, K. E., & Lee, T. 2001, *ApJ*, 548, 1051
- Grosso, N., Feigelson, E. D. et al., 2005, *ApJS*, this issue.
- Güedel, M., Guinan, E. F., & Skinner, S. L. 1997, *ApJ*, 483, 947
- Güedel, M., Audard, M., Smith, K. W., Behar, E., Beasley, A. J., & Mewe, R. 2002, *ApJ*, 577, 371
- Güedel, M., Audard, M., Kashyap, V. L., Drake, J. J., & Guinan, E. F. 2003, *ApJ*, 582, 423
- Güedel, M., Audard, M., Reale, F., Skinner, S. L., & Linsky, J. L. 2004, *A&A*, 416, 713
- Güedel, M. 2002, *ARA&A*, 40, 217
- Güedel, M. 2004, *A&A Rev.*, 12, 71
- Hartmann, L. 1998, *Accretion processes in star formation*, Cambridge Univ. Press
- Hartmann, L. 2001, *Royal Society of London Philosophical Transactions Series A*, 359, 2049
- Hillenbrand, L. A. & Carpenter, J. M. 2000, *ApJ*, 540, 236
- Hillenbrand, L. A. & White, R. J. 2004, *ApJ*, 604, 741

- Hillenbrand, L. A. 1997, *AJ*, 113, 1733
- Hudson, H. S. 1991, *Sol. Phys.*, 133, 357
- Igea, J. & Glassgold, A. E. 1999, *ApJ*, 518, 848
- Jones, B. F. & Walker, M. F. 1988, *AJ*, 95, 1755
- Kastner, J. H., Zuckerman, B., Weintraub, D. A., & Forveille, T. 1997, *Science*, 277, 67
- Krucker, S., & Benz, A. O. 1998, *ApJ*, 501, L213
- Kunz, M. W. & Balbus, S. A. 2004, *MNRAS*, 348, 355
- Lee, T., Shu, F. H., Shang, H., Glassgold, A. E. & Rehm, K. E. 1998, *ApJ*, 506, 898
- Leya, I., Halliday, A. N., & Wieler, R. 2003, *ApJ*, 594, 605
- Leya, I., Halliday, A. N. & Wieler, R. 2003, *ApJ*, 594, 605
- Lin, R. P., et al. 2003, *ApJ*, 595, L69
- Lu, E. T., & Hamilton, R. J. 1991, *ApJ*, 380, L89
- Maloney, P. R., Hollenbach, D. J. & Tielens, A. G. G. M. 1996, *ApJ*, 466, 561
- Marhas, K. K., Goswami, J. N. & Davis, A. M. 2002, *Science*, 298, 2182
- Matsumura, S. & Pudritz, R. E. 2003, *ApJ*, 598, 645
- Micela, G., Sciortino, S., Serio, S., Vaiana, G. S., Bookbinder, J., Golub, L., Harnden, F. R., & Rosner, R. 1985, *ApJ*, 292, 172
- Montmerle, T., Koch-Miramond, L., Falgarone, E., & Grindlay, J. E. 1983, *ApJ*, 269, 182
- Najita, J., Carr, J. S., & Mathieu, R. D. 2003, *ApJ*, 589, 931
- Nakamoto, T., Hayashi, M. R., Kita, N. T, Tachibana, S., 2005, in *Chondrites and the Protoplanetary Disk*, A. Krot et al. eds., (San Francisco: ASP) in press.
- Norman, J. P., Charbonneau, P., McIntosh, S. W., & Liu, H.-L. 2001, *ApJ*, 557, 891
- Osten, R. A., & Brown, A. 1999, *ApJ*, 515, 746
- Osten, R. A., et al. 2004, *ApJS*, 153, 317
- Pallavicini, R., Tagliaferri, G., & Stella, L. 1990, *A&A*, 228, 403

- Parnell, C. E., & Jupp, P. E. 2000, *ApJ*, 529, 554
- Preibisch, T., Kim Y. -C. et al., *ApJS*, this issue (COUP Origins paper)
- Preibisch, T., Feigelson E. D. et al., *ApJS*, this issue (COUP X-ray evolution paper)
- Preibisch, T. 1997, *A&A*, 320, 525
- Reames, D. V., Dennis, R. B., Stone, R. G., & Lin, R. P. 1988, *ApJ*, 327, 998
- Saar, S. H., & Bookbinder, J. A. 1998, in 10th Workshop on Cool Stars, Stellar Systems and the Sun, eds. R. A. Donahue & J. A. Bookbinder, (San Francisco: ASP) 154, 1560
- Sanz-Forcada, J., Brickhouse, N. S., & Dupree, A. K. 2003, *ApJS*, 145, 147
- Scargle, J. D. 1998, *ApJ*, 504, 405
- Semenov, D., Wiebe, D., & Henning, T. 2004, *A&A*, 417, 93
- Semenov, D., Wiebe, D. & Henning, Th. 2004, *A&A*, 417, 93
- Shang, H., Glassgold, A. E., Shu, F. H., & Lizano, S. 2002 *ApJ*, 564, 853
- Shu, F. H., Najita, J. R., Shang, H., & Li, Z.-Y. 2000, in *Protostars and Planets IV*, eds V. Mannings et al., (Tucson: Univ. Arizona Press), 789
- Shu, F. H., Shang, H., Gounelle, M., Glassgold, A. E., & Lee, T. 2001, *ApJ*, 548, 1029
- Sicilia-Aguilar, A., et al., 2005, *AJ*, 129, 363
- Stelzer, B. & Neuhäuser, R. 2001, *A&A*, 377, 538
- Stern, R. A., Schmitt, J. H. M. M., Pye, J. P., Hodgkin, S. T., Stauffer, J. R., & Simon, T. 1994, *ApJ*, 427, 808
- Stone, J. M., Gammie, C. F., Balbus, S. A., & Hawley, J. F. 2000, in *Protostars and Planets IV*, eds V. Mannings et al., (Tucson: Univ. Arizona Press), 589
- Vuong, M. H., Montmerle, T., Grosso, N., Feigelson, E. D., Verstraete, L., & Ozawa, H. 2003, *A&A*, 408, 581
- Walter, F. M., & Barry, D. C. 1991, *The Sun in Time*, 633
- Walter, F. M. & Kuhi, L. V. 1981, *ApJ*, 250, 254
- Wheatland, M. S. 2000, *ApJ*, 536, L109

Wolk, S. J., et al. 2004, ApJ, 606, 466

Figure 1 is not available in the astro-ph version

Fig. 1.— The locations of the Solar mass stars in Orion. A- The Coup image of the ONC 17' on a side (Blue = 2.8-8 keV, Green 1.7-2.8 keV, Red= 0.5-1.7 keV). Locations of Solar mass stars are circled. The two solar analogs not detected are noted with “JW”. B - The 2MASS image of the central 12' of the ONC (Blue = J band, Green = H band, Red= K_s band). Locations of Solar mass stars are circled.

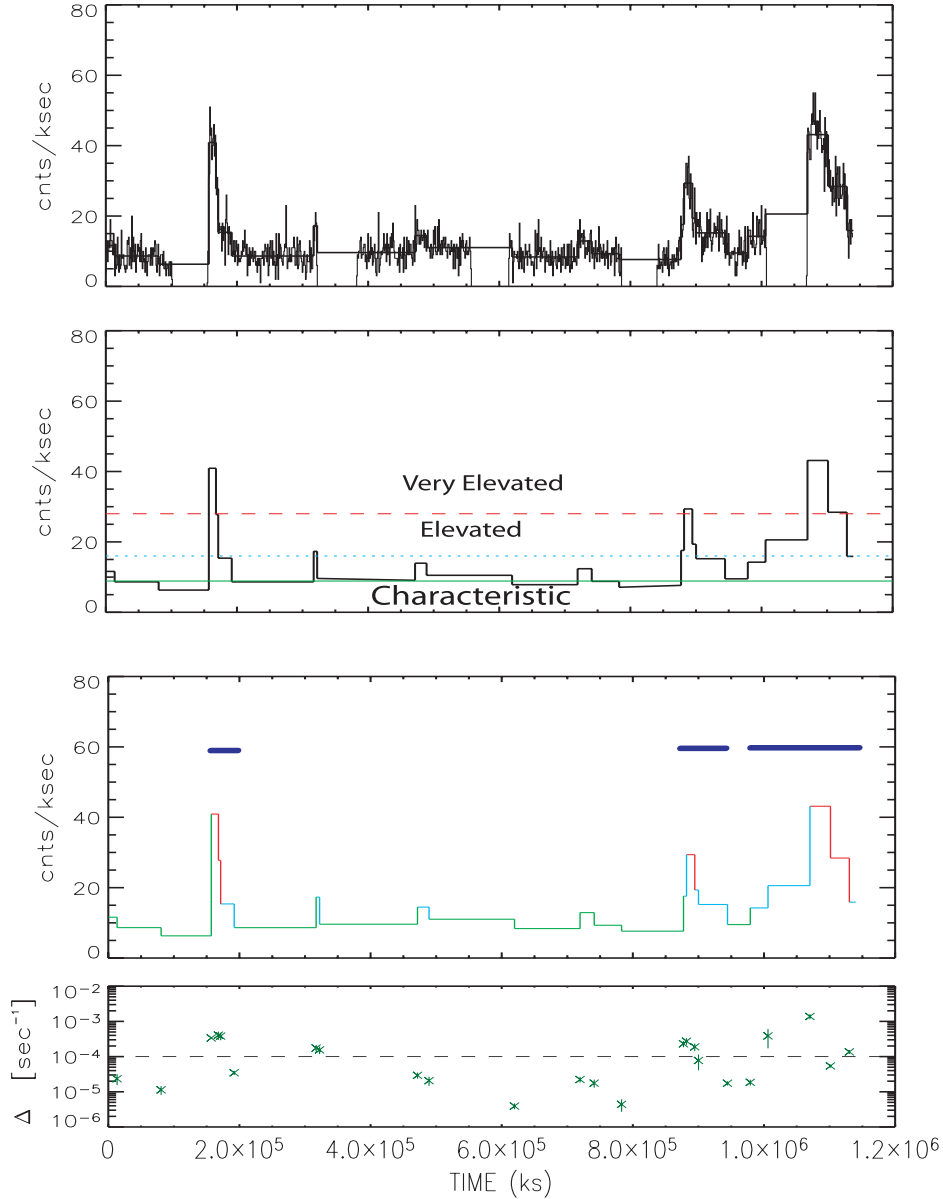


Fig. 2.— Definition of variability levels in a lightcurve of a typical solar-mass COUP source. Top: the lightcurve, represented by a histogram with 1 hour time bins, is converted to blocks of constant flux. Second panel: The characteristic level is determined as shown by the green solid line. The elevated level is marked by the dotted cyan line. The very elevated level is marked by the red dashed line. Every block below the elevated line is grouped with the characteristic blocks. Every block above the very elevated line is in the very elevated group, the remaining blocks are considered elevated. Third Panel: Blocks are colored as in the second panel. Flares as determined in the bottom panel are indicated by the blue lines. Bottom: The rate of change $1/R_{char} \times dR/dt$ is calculated for each block interface, for this case, all three excursions into the very elevated regime are accompanied by rapid changes and are thus considered flares. Note that some rapid changes are not accompanied by high flux rates and thus are not considered to be flares.

Figure 3 is not available in the astro-ph version

Fig. 3.— COUP lightcurves for the 28 solar-mass Orion Nebula Cluster stars. COUP source numbers appear above the plots. The top panel shows the 0.5 – 8 keV brightness variations with bin sizes ranging from 1 ks to 10 ks. Binning is for display only was not used in the analysis. Horizontal lines show the MLB segments. In the electronic version, these are colored green, cyan and red for characteristic, elevated and very elevated segments, respectively. The horizontal blue lines above some red regions indicates periods of flare levels. The lower plot in each panel shows the rate of change between adjacent segments with a dashed line indicating the criterion for flares. The abscissa of all plots show time in seconds from the beginning of the COUP observation. The observation is 13.2 days long with five gaps due to *Chandra* orbit perigees.

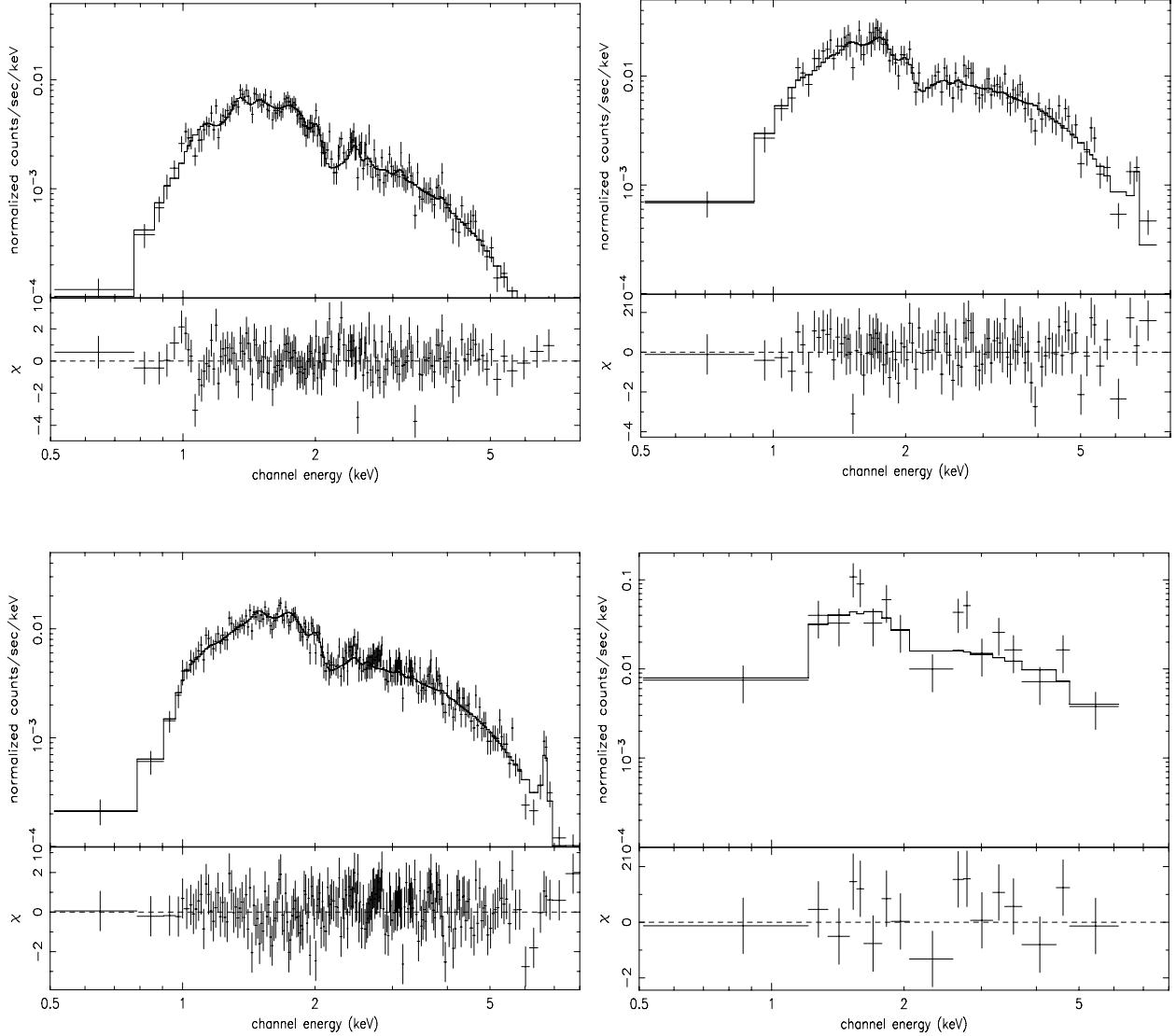


Fig. 4.— An example of fitted spectra of COUP # 262 with N_{H} fixed to $1.6 \times 10^{21} \text{cm}^{-2}$ (in the text it is a free parameter). Upper left: photons which arrived during the characteristic period ($kT_1 = 3.49 \text{eV}$, $kT_2 = 3.51 \text{keV}$). Upper right – photons which arrived during the elevated period ($kT_1 = 80 \text{eV}$, $kT_2 = 5.96 \text{keV}$). Lower left – photons which arrived during the flare ($kT_1 = 80 \text{eV}$, $kT_2 = 8.64 \text{keV}$). Lower right – photons which arrived during the peak flux block of the flare ($kT = 27.1 \text{keV}$). All fits are two temperature MEKAL fits except for the lower right.

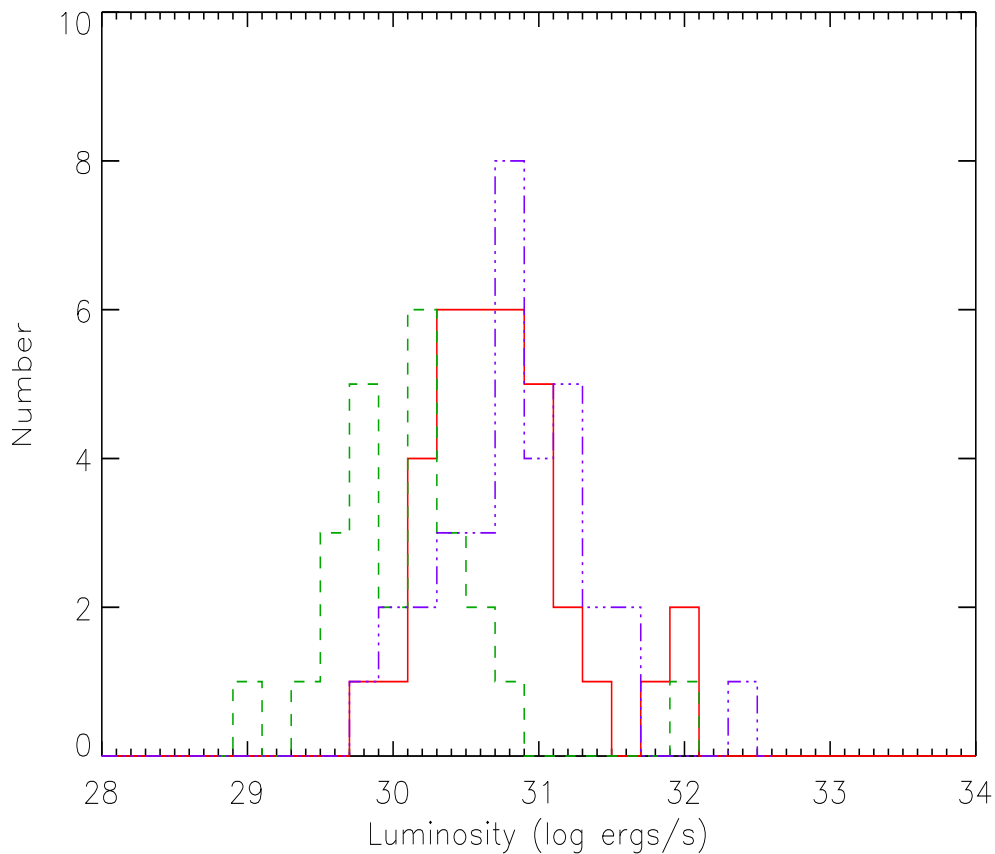


Fig. 5.— Histograms of the characteristic (dashed line), composite flare (solid line) and peak flare (dash-dotted line) luminosities of Solar mass stars in the ONC; Only data with N_{H} fixed to $1.6 A_v \times 10^{21} \text{ cm}^{-2}$ are plotted. The characteristic luminosities are relatively evenly distributed across two orders of magnitude, centered near $\log L_{\text{char}} \sim 30$. The flare luminosities are more sharply peaked near $\log L_{\text{flare}} \sim 30.5$. The peak flare luminosities are centered near $\log L_{\text{flare}} \sim 31$.

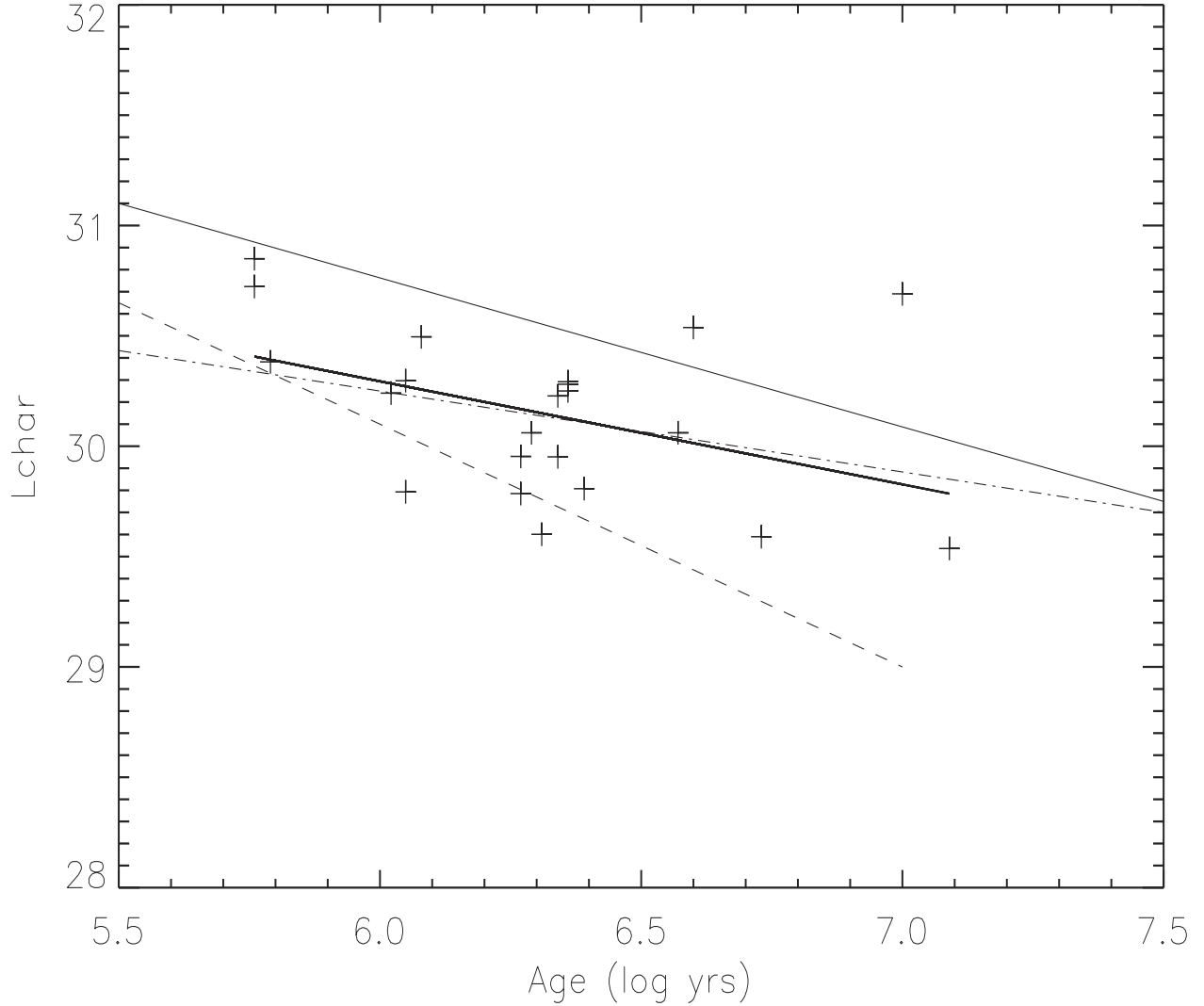


Fig. 6.— Characteristic X-ray luminosity of Solar mass stars in Orion as a function of age. The dashed trend line is adapted from FGP02 and the thick solid trend line is an outlier-resistant two-variable linear regression to the data presented here. The dot-dashed and thin solid lines are taken from Preibisch & Feigelson (2005) Figure 1 for mass ranges of $0.4\text{--}1M_{\odot}$ and $1\text{--}2M_{\odot}$. The $0.4\text{--}1M_{\odot}$ mass range matches the fit derived here.

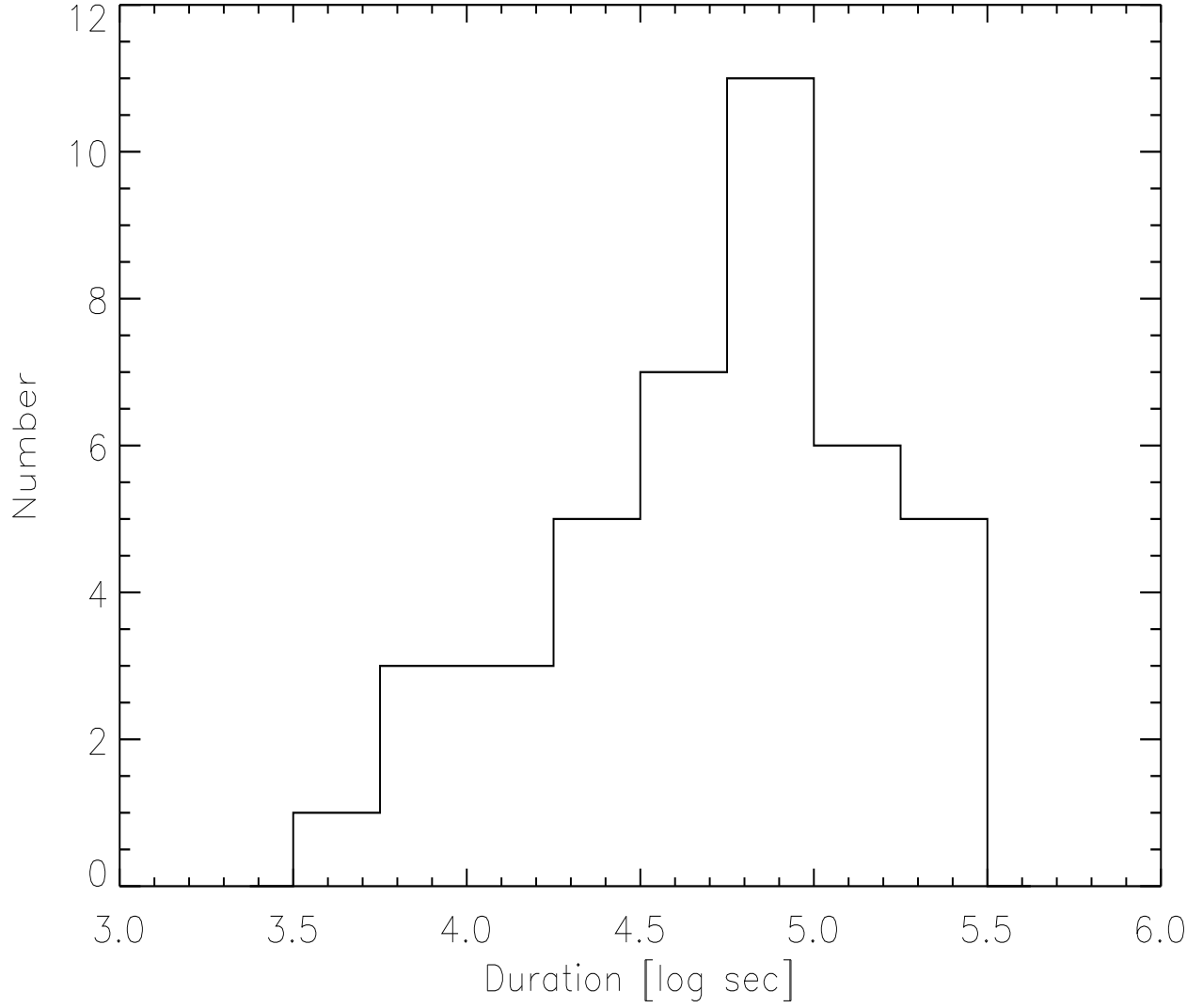


Fig. 7.— Distribution of the duration the “whole flare,” (see text) for all 41 flares.

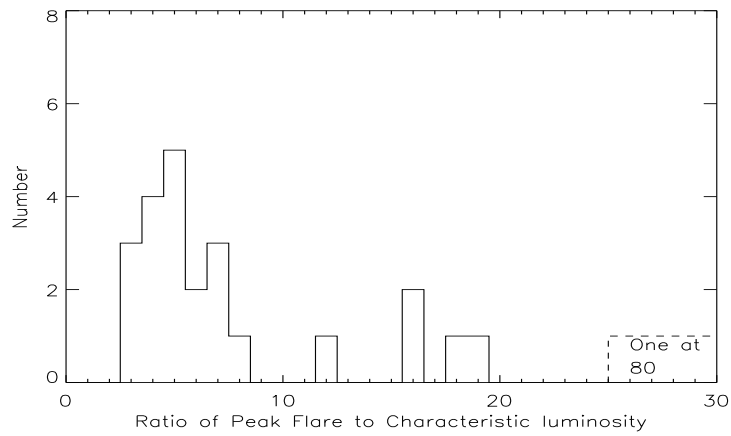
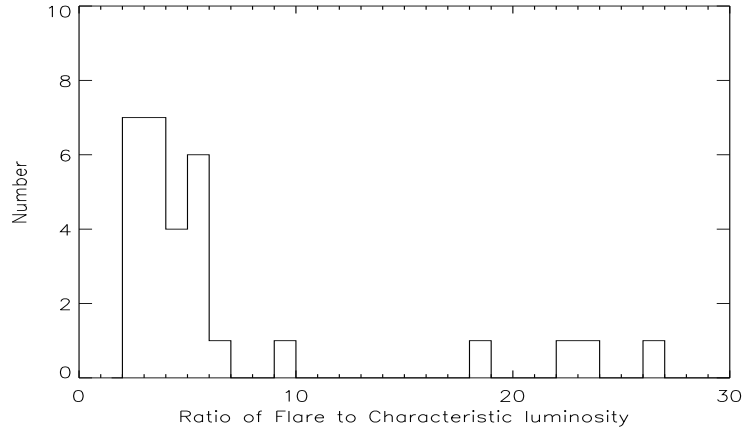


Fig. 8.— Strength of flares. Top: Ratio of the **average** luminosity of each flare to the characteristic level for that star, using the “whole flare” criterion (see text). Bottom: Ratio of the **peak** luminosity for each flare to the characteristic level for that star. Fewer sources are plotted in the shown plot because the “peak flare” criterion sometimes yields insufficient counts for a reliable fit.

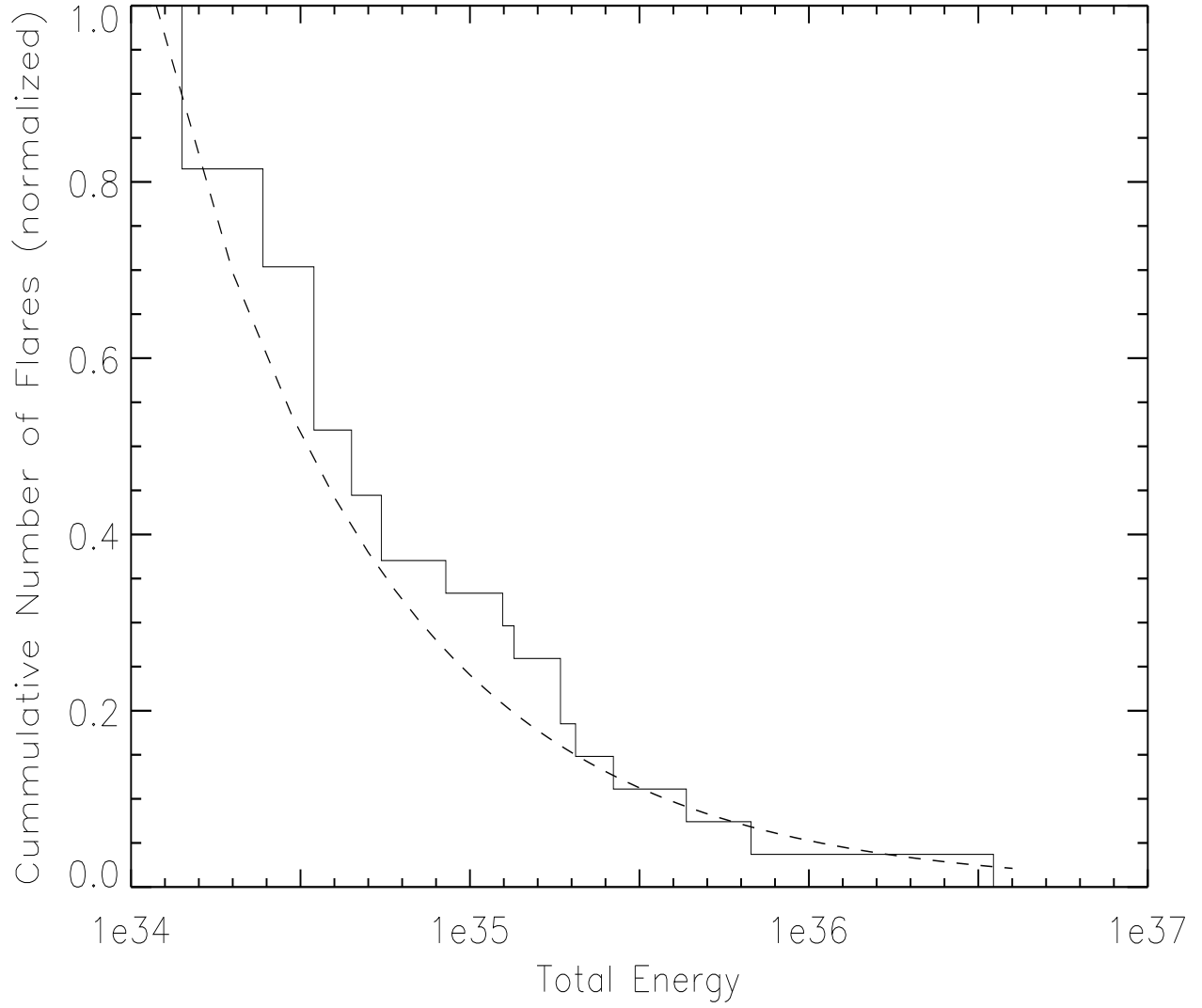


Fig. 9.— Cumulative distribution of flare energy for 27 flares with good spectral fits. The dashed line is the best fit curve $N=1.1 \log E^{-0.66}$.

Figure 10 is not available in the astro-ph version

Fig. 10.— Simulated lightcurves for various power law spectra for the count rate of flares. Two values for the total number of flares are shown. The figures show the resultant lightcurves. The short (red) lines indicate the individual flares. Overall, the simulated lightcurves are remarkably similar to the actual observed light curves. Power laws between -2 and -2.5 seem most similar to the observed data.

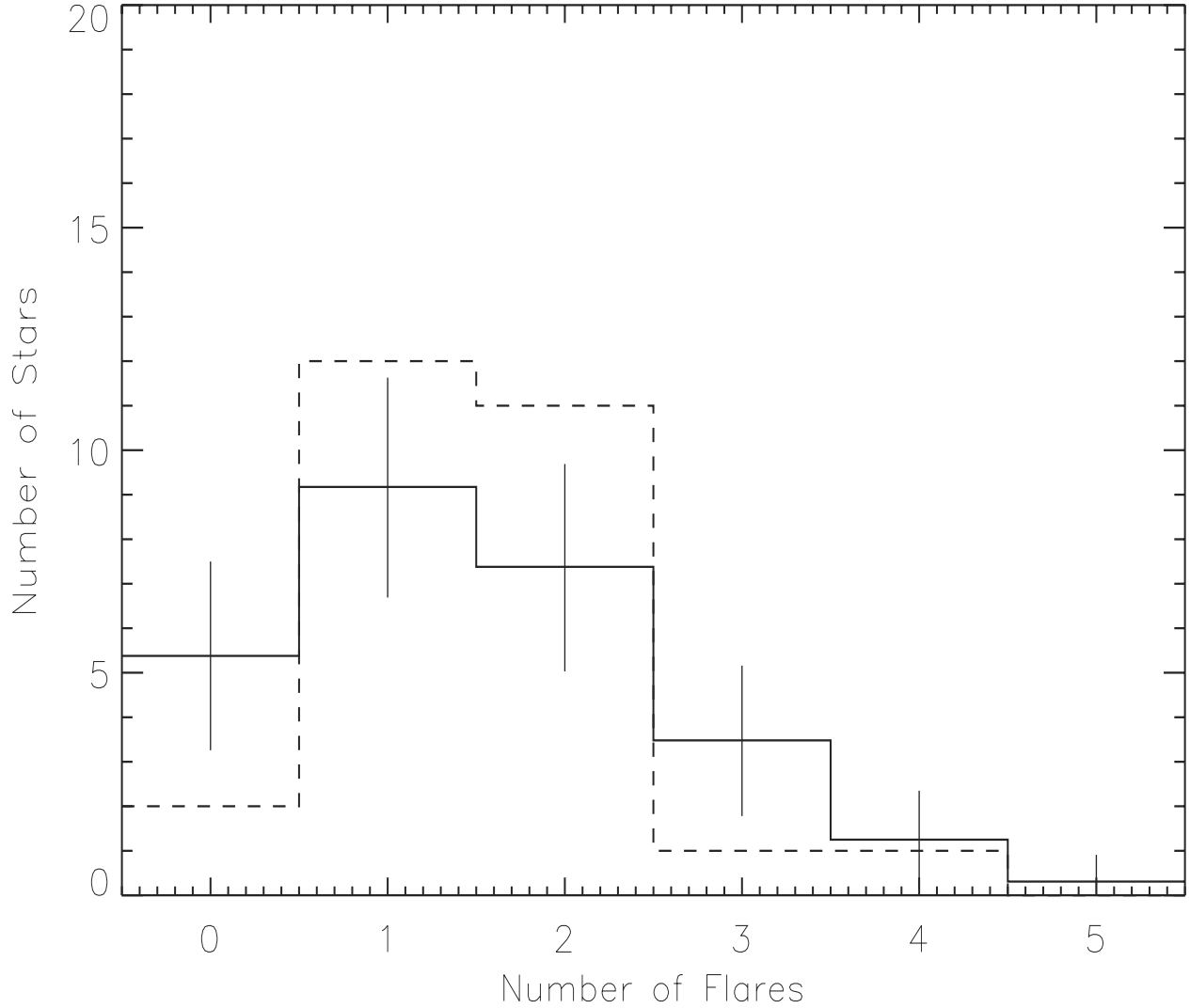


Fig. 11.— Distribution of flare frequency. The solid histogram shows the expected flare distribution if flaring is a random process occurring once per 635 ks. The vertical lines show the standard deviation observed in 1000 simulations. The true distribution is shown by the dashed histogram. The difference between the two distributions is not statistically compelling.

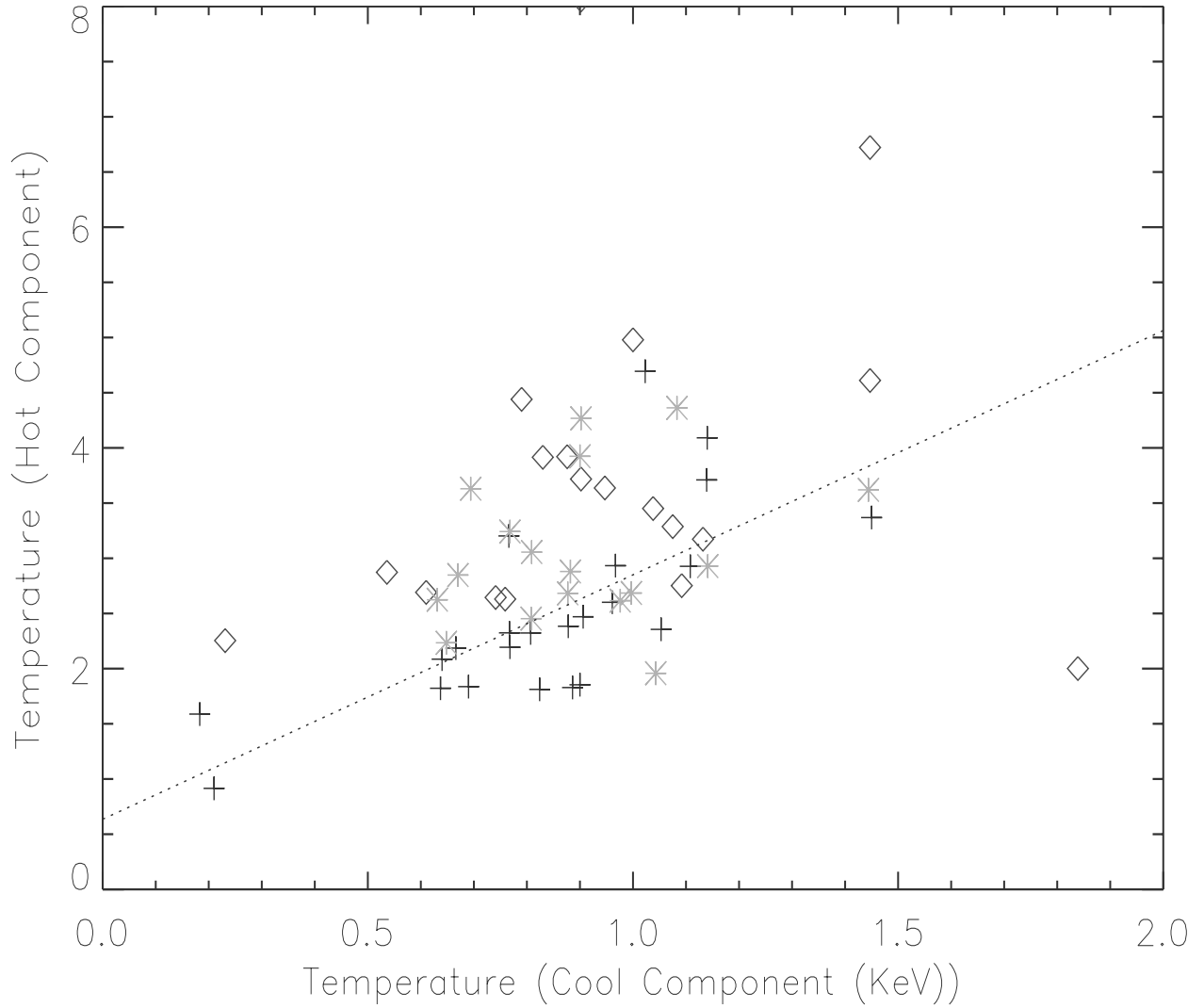


Fig. 12.— Scatter plot of the temperature of the hot coronal component versus the cool component. += characteristic, *= elevated, diamond = average of each flare. The dotted line is a fit to the characteristic data which are well correlated. Coronal components at elevated and flare levels are not correlated.

Table 1. Near-infrared and Optical Properties of Solar Mass Orion Nebula Cluster Stars

COUP	COUP J	JW ^a	offset(")		V	I	J	H	K _s	L	Spec.Type	A _V
			Optical	2MASS								
17	053443.0-052007	63	1.37	1.13	14.81	12.75	11.17	10.37	10.09	—	K6	1.58
54	053450.4-052020	113	0.03	0.43	16.43	14.20	11.96	11.03	10.44	—	K6	2.02
57	053450.7-052401	116	0.09	0.34	13.56	12.12	11.01	10.53	10.28	—	K5	0.33
131	053458.8-052117	187	0.29	0.19	17.12	14.27	11.98	10.95	10.24	—	K5	3.95
147	053500.4-052514	198	0.15	0.21	15.43	13.80	12.19	11.19	10.40	—	K6	0.48
177	053502.4-052046	223a	0.08	0.19	16.06	13.64	11.54	10.52	10.10	—	K5	2.85
223	053504.7-051742	253	0.32	0.23	17.35	14.22	11.53	10.10	9.34	—	K5	4.66
241	053505.4-052717	268	0.14	0.12	14.49	12.88	11.8	11.08	10.84	—	K5-K6	0.43
250	053505.7-052418	278	0.22	0.22	15.6	13.66	11.62	10.30	9.33	8.19	K2-K7	1.61
262	053506.2-052202	286	0.12	0.18	17.69	14.91	11.66	10.07	9.30	8.59	K5	3.77
314	053508.4-052829	320	0.18	0.24	17.1	14.73	13.27	11.78	10.82	—	K2	3.52
515	053513.0-052030	394	0.20	0.23	18.82	14.98	12.29	10.96	10.43	10.09	K6	6.15
567	053513.6-053057	421	0.07	0.26	12.94	11.48	10.18	9.26	8.62	—	K5 ^b	0.38
753	053515.9-051459	487	0.16	0.21	14.57	12.79	11.63	10.77	10.32	—	K6	0.87
828	053516.7-052404	526b	0.35	0.16	13.77	11.87	10.01	9.18	8.89	8.84	K2-K6	1.17
1023	053519.2-052250	9250	0.64	0.19	17.03	14.23	11.98	10.86	10.36	9.88	K5	3.82
1127	053521.0-051637	664	0.14	0.23	16.93	14.05	12.08	11.03	10.64	—	K5.5-7	3.69
1134	053521.0-053121	673	0.17	0.30	14.9	13.07	11.57	10.62	10.03	—	K5	1.33
1151	053521.3-052644	683	0.10	0.21	13.61	11.76	10.48	9.64	9.40	—	K6	1.05
1167	053521.7-052339	694	0.29	0.23	17.73	14.74	12.54	11.42	10.80	9.83	K5-K7	3.97
1235	053522.9-052241	726	0.23	0.20	19.24	15.35	12.5	11.03	10.33	9.95	K5-K7	6.28
1259	053523.6-052331	738	0.15	0.18	15.7	13.84	11.97	10.92	10.45	10.09	K5	1.41
1281	053524.2-052518	750	0.28	0.03	14.85	12.87	11.53	10.54	9.94	9.25	K0-K5	1.72
1326	053525.4-052134	777	0.64	0.02	18.46	15.15	12.72	11.40	10.58	—	K6	4.79
1327	053525.4-052135	777	0.59	0.02	18.46	15.15	12	10.90	10.53	9.86	K6	4.79
1500	053532.9-051605	892	0.18	0.30	16.21	13.99	11.62	10.49	10.06	—	lateK	2.00
1539	053537.5-052716	930	0.03	0.06	16.64	14.08	12.71	11.94	11.71	—	K5-K7	2.87
1570	053542.4-052733	962	0.08	0.05	15.23	13.26	11.39	10.57	10.12	—	K6	1.35

^aJones, B. F. & Walker, M. F. 1988, AJ, 95, 1755

^bHillenbrand (1997) list this as a K5 (as measured by Hillenbrand) with a previous spectral type of F8-G0III-IV with an unknown reference

Table 2. Inferred properties of Solar Mass Stars

COUP	$\log T_{eff}$ (K)	$\log L_{bol}$ (ergs s^{-1})	Radius R_{\odot}	Mass M_{\odot}	\log Age (Yrs)	$\Delta(I - K)$ mag.	EW Ca \AA	Notes
17	3.62	0.26	2.57	0.90	6.05	0.20	1.9	d
54	3.62	-0.21	1.49	0.92	6.73	1.20	-1.0	b
57	3.64	0.20	2.17	1.19	6.36	0.09	1.6	d
131	3.64	0.22	2.23	1.20	6.34	0.53	1.4	b
147	3.62	-0.43	1.16	0.90	7.09	1.96	-1.0	b,c
177	3.64	0.20	2.18	1.19	6.36	0.48	2.0	b
223	3.64	0.41	2.79	1.19	6.08	1.04	1.7	b
241	3.62	-0.07	1.75	0.93	6.50	0.16	2.8	d
250	3.64	-0.11	1.53	1.12	6.82	1.69	-9.6	a
262	3.64	-0.08	1.58	1.13	6.78	2.24	2.3	b
314	3.70	-0.08	1.25	1.10	7.28	0.98	0.3	b
515	3.62	0.49	3.32	0.90	5.79	-0.20	0.0	d
567	3.64	0.47	2.96	1.20	6.02	0.80	-3.5	a
753	3.62	0.07	2.06	0.91	6.29	0.28	1.8	d
828	3.62	0.52	3.43	0.90	5.76	0.74	1.2	b,e
1023	3.64	0.20	2.19	1.19	6.36	0.13	0.6	d
1127	3.62	0.26	2.55	0.90	6.05	-0.18	1.4	d,f
1134	3.64	0.06	1.86	1.17	6.57	0.81	1.3	b
1151	3.62	0.53	3.48	0.91	5.76	0.28	1.9	d
1167	3.62	0.05	2.01	0.91	6.32	0.18	-3.8	a,c
1235	3.62	0.37	2.90	0.90	5.92	0.17	0.0	d
1259	3.64	-0.23	1.33	1.05	7.00		-0.3	
1281	3.64	0.24	2.27	1.20	6.31	0.38	0.0	b,c
1326	3.62	0.09	2.09	0.91	6.27	1.03	2.5	b
1327	3.62	0.09	2.09	0.91	6.27	1.03	2.5	b
1500	3.62	-0.13	1.63	0.94	6.60		1.0	
1539	3.62	0.04	2.00	0.92	6.34	-0.71	5.2	d
1570	3.62	0.00	1.90	0.92	6.39	0.80	1.8	b

^aAccreting disk

^bDisk - no evidence of accretion

^cProplyd (Hillenbrand 1997)

^dNo evidence of a disk

^eJW 526a & 526b

^fJW 892 & 3018

Table 3. Time-averaged X-ray Luminosity of Solar Mass Stars

COUP	NetCnts	$\log L_s^a$	$\log L_h^a$	$\log L_t^a$	$\log L_{t,c}^a$	Notes
17	1083	29.67	29.72	29.99	30.07	c,g
54	1583	29.36	29.26	29.61	29.86	
57	4093	30.28	29.89	30.43	30.48	b
131	9038	29.96	30.34	30.49	30.77	b,h
147	2348	29.51	29.41	29.76	29.90	b,g
177	5054	29.79	29.82	30.11	30.41	h
223	10243	30.00	30.51	30.62	31.08	h
241	314	27.85	29.24	29.26	29.94	
250	497	28.57	29.16	29.26	29.45	
262	11540	30.06	30.61	30.72	31.15	h
314	458	28.27	29.34	29.38	29.96	
515	4393	29.66	29.94	30.12	30.57	g,h
567	10847	30.18	30.16	30.47	30.59	b
753	5729	29.87	29.98	30.23	30.43	
828	12067	30.57	30.89	31.06	31.20	d,f
1023	4852	29.70	29.95	30.14	30.53	f
1127	5598	29.84	29.95	30.20	30.53	g
1134	4922	29.92	29.74	30.14	30.21	g
1151	24094	30.53	30.41	30.77	30.85	g,h
1167	335	28.30	29.16	29.22	29.90	f
1235	345	28.92	29.27	29.43	29.71	b,d
1259	2183	30.73	30.79	31.06	31.26	e
1281	1554	29.31	29.25	29.58	29.72	f
1326	714	29.18	29.38	29.60	29.84	b,h
1327	1003	29.35	29.55	29.76	30.04	b,h
1500	4438	30.20	30.50	30.68	30.95	b,c,g
1539	1210	29.33	28.75	29.43	29.43	
1570	4146	29.70	29.91	30.12	30.33	g

^aThe logarithm of the luminosity in units of ergs s^{-1} .

^bDouble sources (percentage of PSF extracted to avoid the neighbor): 57 (32%), 131 (87%), 147 (87%), 567 (88%), 1259 (N/A), 1326 (44%), 1327 (43%), 1500 (67%). 1326+1327 are a pair of solar analogs (as the text notes) while the other companions have different or unknown masses.

^cPSF extends over detector edge, the effect is minor and can be ignored.

^dNear a chip gap, the effect is significant for 828.

^eSuffers pileup only outer 7% of photons are analyzed.

^fSuffers background contamination (usually PSF wings of θ^1 Ori C). This is unimportant as our sources are very strong.

^gExhibits Ne/Fe spectral line abundance anomalies around 0.8-1.3.

^hSpectral lines in the 1.3 keV region.

Table 4. Spectral Fits to Characteristic X-ray Flux

COUP	Duration (sec)	nbins	χ^2/df	$\log P$	N_{H} ($\times 10^{21} \text{ cm}^{-2}$)	KT1 (keV)	KT2 (keV)	E.M. Ratio (EM1/EM2)	$\log L_{t,c}$ (ergs s^{-1})	$\log E$ (ergs)	Notes
17	549316	28	1.9	-2.4	0.40	1.02	4.69	1.57	29.79	35.53	
54	650772	49	1.0	-0.4	0.51	0.67	2.19	1.14	29.59	35.40	
57	735173	99	1.3	-1.5	0.08	0.69	1.84	0.72	30.28	36.15	
131	396531	93	1.0	-0.4	1.01	0.88	2.38	0.31	30.23	35.83	
147	523161	48	1.2	-0.8	0.13	0.77	3.20	0.20	29.54	35.26	
177	789112	138	1.2	-1.0	0.74	0.77	2.19	0.60	30.25	36.15	
223	578569	153	1.3	-1.9	1.20	1.05	2.36	0.19	30.50	36.26	
241	744731	18	1.5	-0.9	7.57	0.08	2.08	>100	33.23	39.10	a
250	556094	18	0.9	-0.2	3.79	0.08	2.40	>100	32.41	38.16	a
262	519007	168	1.0	-0.5	3.46	0.18	1.59	54.83	32.28	38.00	a
314	586693	16	1.4	-0.8	5.94	0.11	2.33	>100	31.96	37.73	a
515	635948	118	1.3	-1.7	1.57	0.77	2.32	1.21	30.38	36.19	
567	625851	153	1.5	—	0.10	0.97	2.93	0.44	30.24	36.04	
753	640962	129	2.0	—	0.22	1.11	2.93	0.27	30.06	35.87	
828	632461	187	1.8	—	0.30	1.14	4.09	0.17	30.85	36.65	
1023	830706	163	1.2	-1.3	0.98	0.91	2.47	0.23	30.29	36.21	
1127	734165	133	1.1	-0.6	0.94	0.82	1.81	0.52	30.30	36.16	
1134	669494	109	1.4	-2.5	0.34	0.64	2.09	0.75	30.06	35.88	
1151	689861	232	1.8	—	0.28	0.81	2.32	0.42	30.72	36.56	
1167	527616	9	1.2	-0.5	1.02	> 15	> 15	0.10	28.96	34.68	
1235	817070	19	1.6	-1.1	1.62	1.50	> 15	15.15	29.66	35.58	
1259	572943	44	0.9	-0.2	0.37	0.89	1.83	0.36	31.85	37.60	
1281	797023	68	1.1	-0.5	0.45	0.96	2.60	0.76	29.60	35.50	
1326	746680	30	1.1	-0.5	1.23	0.64	1.82	0.33	29.79	35.66	
1327	825748	48	1.0	-0.3	1.23	0.90	1.85	0.39	29.95	35.87	
1500	618698	109	1.9	—	0.51	1.45	3.37	0.05	30.54	36.33	
1539	757046	38	1.2	-0.6	0.74	0.21	0.92	10.09	29.95	35.83	
1570	561651	75	1.6	-3.0	0.35	1.14	3.71	0.27	29.81	35.56	

^aHydrogen column N_{H} was fit as a free parameter.

Table 5. Spectral Fits to Elevated X-ray Flux

COUP	Duration (sec)	nbins	χ^2/df	$\log P$	N_{H} ($\times 10^{21} \text{ cm}^{-2}$)	KT1 (keV)	KT2 (keV)	E.M. Ratio (EM1/EM2)	$\log L_{t,c}$ (ergs s^{-1})	$\log E$ (ergs)	Notes
17	204741	26	1.06	-0.4	0.40	0.90	3.92	0.50	30.22	35.54	
54	35090	15	1.54	-1.0	0.51	0.65	2.23	0.31	29.83	34.38	
57	42944	34	0.82	-0.1	0.08	0.81	3.06	3.06	30.60	35.23	
131	99546	106	0.93	-0.2	1.01	0.88	2.68	0.63	30.53	35.53	
147	231582	50	0.93	-0.2	0.13	0.67	2.85	0.11	29.85	35.22	
177	52790	33	1.06	-0.4	0.74	0.90	4.27	0.45	30.51	35.24	
223	32474	116	1.21	-1.2	1.20	1.14	2.93	0.30	30.73	35.24	
262	76306	187	1.03	-0.4	2.33	0.98	2.62	0.48	31.15	35.03	a
515	131208	68	1.28	-1.2	1.57	0.81	2.45	0.27	30.61	35.72	
567	22858	95	1.30	-1.5	0.10	1.08	4.36	2.15	30.51	34.87	
753	61711	91	1.55	-3.0	0.22	1.44	3.62	0.12	30.33	35.13	
828	158275	176	1.13	-0.9	0.30	12.09	3.71	0.45	31.23	36.43	
1023	18806	17	0.49	0.0	0.98	0.69	3.63	0.04	30.59	34.87	
1127	22663	43	1.08	-0.5	0.94	1.04	1.96	2.66	30.50	34.86	
1134	75494	49	1.44	-1.6	0.34	0.63	2.62	0.80	30.33	35.21	
1151	132262	169	1.16	-1.1	0.27	0.88	2.88	0.00	30.94	36.06	
1259	65114	13	0.66	-0.1	0.37	2.23	2.29	0.32	30.99	35.80	
1281	52489	13	0.65	-0.1	0.45	0.77	3.24	0.67	30.01	34.73	
1326	72598	12	1.24	-0.6	1.23	1.24	78.41	0.45	30.09	34.95	
1500	15234	64	1.83	—	0.51	0.08	6.14	0.23	30.90	35.08	
1570	65831	31	1.16	-0.6	0.35	1.00	2.69	0.00	30.13	34.95	

^aHydrogen column N_{H} was fit as a free parameter.

Table 6. Spectral Fits to Integrated Flares

COUP	Flare #	Duration (sec)	nbins	χ^2/df	$\log P$	N_{H} ($\times 10^{21} \text{ cm}^{-2}$)	KT1 (keV)	KT2 (keV)	E.M. Ratio (EM1/EM2)	$\log L_{t,c}$ (ergs s^{-1})	$\log E$ (ergs)	Notes
17	1	44113	13	1.26	-0.6	0.40	0.90	4.37	0.19	30.46	35.11	a
54	1	9067	10	1.90	-1.1	0.51	0.08	2.08	0.35	30.55	34.51	a
54	2	154578	35	0.62	0.0	0.51	0.61	2.69	>100	30.07	35.26	b
57	1	58063	34	1.24	-0.8	0.08	0.88	3.92	0.30	30.77	35.53	a
57	2	13326	15	0.76	-0.2	0.08	0.72	> 15	0.73	30.99	35.12	b
131	1	190371	134	0.95	-0.2	1.01	0.18	3.06	>100	30.81	36.09	b
131	2	163058	154	0.90	-0.1	1.01	0.90	3.72	0.11	30.92	36.13	b
147	1	24873	11	0.92	-0.3	0.13	0.76	2.55	0.45	29.90	34.30	g
147	2	7864	11	1.24	-0.6	0.13	1.14	> 15	0.28	30.25	34.15	c,g
177	1	7604	15	0.79	-0.2	0.74	0.90	8.06	0.35	30.86	34.74	a
223	1	173205	173	0.99	-0.3	1.20	0.08	4.77	0.00	31.02	36.25	a
223	2	65264	96	1.40	-2.2	1.20	0.08	9.56	0.37	31.11	35.92	a
241	1	104787	14	0.56	-0.1	11.26	0.08	1.59	>100	35.18	40.20	b,g
250	1	246439	16	0.79	-0.2	2.96	0.09	2.10	>100	32.15	37.54	a,g
262	3	254193	214	0.95	-0.2	2.29	1.13	3.17	3.28	31.23	36.63	a,g
314	1	99223	13	1.26	-0.6	4.94	0.13	2.61	>100	31.87	36.86	a,g
314	2	14226										c,e
314	3	131465	11	1.03	-0.4	20.34	0.08	0.58	>100	37.56	42.68	b,c,f
314	4	17910										a,e
515	1	82357	54	0.90	-0.2	1.57	0.76	2.63	0.38	30.79	35.70	a
567	1	34980	50	1.14	-0.6	0.83	0.79	4.44	0.41	30.96	35.50	a
567	2	67095	66	1.25	-1.0	0.10	1.00	4.98	0.19	30.60	35.43	a,i
567	3	98734	112	0.96	-0.2	0.20	1.04	3.45	0.41	30.74	35.73	b
753	1	80367	43	1.55	-1.8	0.22	1.45	4.61	0.21	30.36	35.26	a
753	2	66472	58	1.12	-0.6	1.63	0.23	2.25	6.31	31.44	36.26	a
1127	1	52594	32	1.28	-0.8	0.94	1.09	2.75	0.10	30.57	35.29	a,h,i
1127	2	40090	60	0.69	0.0	0.94	0.54	2.87	0.55	31.03	35.63	a
1134	1	19758	16	0.87	-0.2	0.37	0.83	3.92	0.96	30.57	34.86	a
1134	2	35233	24	0.67	-0.1	0.37	0.74	2.65	0.31	30.48	35.03	a
1151	1	27396	69	1.19	-0.9	0.27	0.95	3.64	0.36	31.03	35.47	b
1167	1	203281	15	0.74	-0.2	5.33	0.72	5.95	5.47	30.38	35.69	a
1235	1	32443										a,e
1259	1	149468	25	1.37	-0.9	0.37	1.84	2.00	0.82	32.40	37.57	b,i
1259	2	61987	62	1.15	-0.7	0.37	1.45	6.72	4.41	33.19	37.98	a
1326	1	4103										c,e
1326	2	26132	13	1.22	-0.6	1.23	0.08	2.32	>100	31.05	35.47	a
1327	1	16381	10	1.98	-1.2	1.23	0.08	4.46	0.00	30.72	34.94	a
1500	1	215580	101	1.78	-	0.51	4.96	> 15	>100	30.97	36.30	a
1539	1	70264	27	1.23	-0.7	0.74	0.20	1.68	7.95	30.76	35.60	a
1570	1	41441	16	0.54	-0.1	0.35	1.08	3.29	0.17	30.21	34.82	a,e
1570	2	94762	64	1.00	-0.3	0.35	4.92	> 15	>100	30.54	35.52	b

^aFlare morphology - Rapid Rise followed by exponential decay.

^bFlare morphology - Symmetric

^cFlare morphology - Spike, Rise and fall within 5ks.

^dFlare morphology - weak irregular.

^eNot enough photons to fit.

^fFormally good fit but very few photons.

^gNearby star may have affected fit.

^hDuration overstated, probably closer to 5 ks.

ⁱHydrogen column N_{H} was fit as a free parameter.

Table 7. Spectral Fits to the Peak of Each Flare

COUP	Flare #	Duration (sec)	nbins	χ^2/df	$\log P$	N_{H} ($\times 10^{21} \text{ cm}^{-2}$)	KT1 (keV)	KT2 (keV)	E.M. Ratio (EM1/EM2)	$\log L_{t,c}$ (ergs s^{-1})	$\log E$ (ergs)
17	1	24133	18	0.82	-0.2	0.40	0.08	2.92	23.57	30.62	35.01
54	1	9066	10	1.90	-1.1	0.51	0.08	2.08	>100	30.55	34.51
54	2	85122	26	0.99	-0.3	0.51	0.50	3.02	0.26	30.20	35.13
57	1	10979	16	0.37	0.0	0.08	0.71	4.77	0.15	31.01	35.05
57	2	13326	15	0.76	-0.2	0.08	0.72	>15	0.30	30.99	35.12
131	1	20013	49	0.99	-0.3	1.01	0.11	4.88	9.85	31.43	35.74
131	2	24266	42	1.05	-0.4	1.01	0.71	4.15	0.17	31.08	35.46
147	1	21775	15	0.63	-0.1	0.13	0.74	>15	0.67	29.98	34.32
147	2	7864	11	1.24	-0.6	0.13	1.14	>15	0.28	30.25	34.15
177	1	1848	14	0.43	0.0	0.74	1.08	>15	0.17	31.20	34.47
223	1	9407	59	1.14	-0.7	1.20	>15	>15	2.57	31.71	35.68
223	2	25817	60	2.06	—	1.20	0.08	>15	0.00	31.28	35.69
250	1	7473	10	2.79	-2.0	0.41	0.08	>15	0.00	30.30	34.18
262	3	965	17	1.38	-0.8	0.96	0.08	>15	0.00	31.60	34.59
314	1	19279	14	3.25	—	0.90	0.08	>15	0.00	30.02	34.31
515	1	18945	23	1.01	-0.3	1.57	1.78	5.47	3.10	30.97	35.25
567	1	10862	27	2.54	—	0.10	0.08	>15	0.00	31.06	35.10
567	2	12673	23	1.17	-0.6	0.10	1.12	6.95	0.14	30.85	34.95
567	3	31332	67	0.85	-0.1	0.10	1.14	3.59	0.34	30.94	35.44
753	1	4022	19	0.80	-0.2	0.22	2.32	>15	0.58	30.82	34.43
753	2	4558	19	3.60	—	0.22	0.08	>15	0.00	31.33	34.99
1127	1	2811	13	0.59	-0.1	0.98	0.75	4.31	0.42	31.00	34.44
1127	2	8231	30	0.72	-0.1	0.98	1.72	5.95	0.52	31.40	35.32
1134	1	6395	13	0.82	-0.2	0.34	0.16	3.03	2.42	30.93	34.74
1134	2	15383	14	1.45	-0.8	0.34	0.71	4.10	0.39	30.60	34.79
1134	3	49539	40	0.66	0.0	0.34	0.65	3.22	0.31	30.59	35.29
1151	1	3078	17	1.21	-0.6	0.27	1.12	>15	0.35	31.40	34.89
1259	1	55286	14	0.36	0.0	0.37	1.55	>15	40.62	31.26	36.01
1259	2	2926	16	2.94	—	0.37	3.26	3.59	12.69	32.60	36.06
1327	1	16380	10	1.98	-1.2	1.23	0.08	4.46	0.00	30.72	34.94
1539	1	32052	16	0.33	0.0	0.74	0.17	1.54	12.89	30.81	35.31
1570	1	8585	15	0.86	-0.2	0.35	1.83	>15	0.60	30.43	34.36
1570	2	4836	17	1.01	-0.4	0.35	9.87	>15	0.00	31.09	34.78